Endothelial Pannexin 1–TRPV4 channel signaling lowers pulmonary arterial pressure

Panx1-TRPV4 signaling in pulmonary endothelium

[1]Zdravka Daneva; [1,2]Matteo Ottolini; [1]Yen-Lin Chen; [1]Eliska Klimentova; [3]Soham A. Shah; [4]Richard D. Minshall; [5]Cheikh I. Seye, [6]Victor E. Laubach; [7]Brant E. Isakson; [1,7]Swapnil K. Sonkusare

[1]Robert M. Berne Cardiovascular Research Center, University of Virginia, Charlottesville, VA, 22908, USA;
[2]Department of Pharmacology, University of Virginia, Charlottesville, VA, 22908, USA;
[3]Department of Biomedical Engineering, University of Virginia, Charlottesville, VA, 22908, USA;
[4]Department of Anesthesiology, University of Illinois at Chicago, Chicago, IL, USA; Department of Pharmacology, University of Illinois at Chicago, Chicago, IL, USA;
[5]Department of Biochemistry, University of Missouri-Columbia, Columbia, MO, USA;
[6]Department of Surgery, University of Virginia, Charlottesville, VA, 22908, USA;
[7]Department of Molecular Physiology and Biological Physics, University of Virginia, Charlottesville, VA, 22908, USA

Correspondence should be addressed to:

Swapnil K. Sonkusare, Ph.D.
University of Virginia School of Medicine
P.O. Box 801394
Charlottesville, VA 22908
E-mail: sks2n@virginia.edu
Phone: 434-297-7401

Key Words: Pannexin 1, TRP channels, pulmonary artery, endothelium, purinergic signaling, caveolin 1.

Abstract.

Pannexin 1 (Panx1) is an ATP-efflux channel that controls endothelial function in the systemic circulation. However, the roles of endothelial Panx1 in resistance-sized pulmonary arteries (PAs) are unknown. Extracellular ATP dilates PAs through activation of endothelial TRPV4 (transient receptor potential vanilloid 4) ion channels. We hypothesized that endothelial Panx1–ATP–TRPV4 channel signaling promotes vasodilation and lowers pulmonary arterial pressure (PAP). Endothelial, but not smooth muscle, knockout of Panx1 or TRPV4 increased PA contractility and raised PAP. Panx1-effluxed extracellular ATP signaled through purinergic P2Y2 receptor (P2Y2R) to activate protein kinase Cα (PKCα), which in turn activated endothelial TRPV4 channels. Finally, caveolin-1 provided a signaling scaffold for endothelial Panx1, P2Y2R, PKCα, and TRPV4 channels in PAs, promoting their spatial proximity and enabling signaling interactions. These results indicate that endothelial Panx1–P2Y2R–TRPV4 channel signaling, facilitated by caveolin-1, reduces PA contractility and lowers PAP.

Introduction

The pulmonary endothelium exerts a dilatory influence on small, resistance-sized pulmonary arteries (PAs) and thereby lowers pulmonary arterial pressure (PAP). However, endothelial signaling mechanisms that control PA contractility remain poorly understood. In this regard, pannexin 1 (Panx1), which is expressed in the pulmonary endothelium and epithelium[1], has emerged as a crucial controller of endothelial function[2, 3]. Panx1, the most studied member of the pannexin family, forms a hexameric transmembrane channel at the cell membrane that allows efflux of ATP from the cytosol[4, 5]. Previous studies have indicated that $Panx1_{EC}$ promotes endothelium-dependent dilation of systemic arteries[6, 7], and endothelial cell (EC) Panx1 ($Panx1_{EC}$) has been linked to inflammation in pulmonary capillaries[8]. Beyond this, however, the physiological roles of $Panx1_{EC}$ in the pulmonary vasculature are largely unknown.

Extracellular ATP (eATP) was recently shown to activate TRPV4 (transient receptor potential vanilloid 4) channels in the endothelium of small PAs[9], establishing endothelial TRPV4 ($TRPV4_{EC}$) channels as potential signaling targets of $Panx1_{EC}$ in the pulmonary circulation. Ca^{2+} influx through $TRPV4_{EC}$ channels is known to dilate small PAs through activation of endothelial nitric oxide synthase (eNOS)[9]. These observations suggest that $Panx1_{EC}$-released eATP may act through $TRPV4_{EC}$ channels to reduce PA contractility and lower PAP.

Purinergic receptor signaling is an essential regulator of pulmonary vascular function[10-13]. Previous studies in small PAs showed that eATP activates $TRPV4_{EC}$ channels through P2 purinergic receptors, although the precise P2 receptor subtype was not identified[9]. Pulmonary endothelium expresses both P2Y and P2X receptor subtypes. Konduri et al. showed that eATP dilates PAs through P2Y2 receptor (P2Y2R) activation and subsequent endothelial NO release[13]. Recent evidence from systemic ECs and other cell types also supports P2Y2R-dependent

activation of TRPV4 channels by eATP[14, 15]. These findings raise the possibility that the endothelial P2Y2 receptor ($P2Y2R_{EC}$) may be the signaling intermediate for $Panx1_{EC}$–$TRPV4_{EC}$ channel communication in PAs.

The linkage between $Panx1_{EC}$-mediated eATP release and subsequent activation of $P2Y2R_{EC}$–$TRPV4_{EC}$ signaling could depend on the spatial proximity of individual elements—$Panx1_{EC}$, $P2Y2R_{EC}$, and $TRPV4_{EC}$—a functionality possibly provided by a signaling scaffold. Caveolin-1 (Cav-1), a structural protein that interacts with and stabilizes other proteins in the pulmonary circulation[16], co-localizes with Panx1, P2Y2R, and TRPV4 channels in multiple cell types[17-19]. Notably, global Cav-$1^{-/-}$ mice show elevated PAP, and endothelial Cav-1 (Cav-1_{EC})-dependent signaling is impaired in pulmonary hypertension[20-22].

Here, we tested the hypothesis that $Panx1_{EC}$–$P2Y2R_{EC}$–$TRPV4_{EC}$ channel signaling, supported by a signaling scaffold provided by Cav-1_{EC}, reduces PA contractility and PAP. Using inducible, EC-specific Panx$1^{-/-}$, TRPV$4^{-/-}$, P2Y$2R^{-/-}$ and Cav-$1_{EC}^{-/-}$ mice, we show that endothelial Panx1–P2Y2R–TRPV4 signaling reduces PA contractility and lowers PAP. $Panx1_{EC}$-generated eATP acts via $P2Y2R_{EC}$ stimulation to activate protein kinase Cα (PKCα) and thereby increase $TRPV4_{EC}$ channel activity. $Panx1_{EC}$, $P2Y2R_{EC}$, PKCα, and $TRPV4_{EC}$ channels co-localize with Cav-1_{EC}, ensuring spatial proximity among the individual elements and supporting signaling interactions. Overall, these findings advance our understanding of endothelial mechanisms that control PAP and suggest the possibility of targeting these mechanisms to lower PAP in pulmonary vascular disorders.

Results

Endothelial, but not smooth muscle, Panx1–TRPV4 signaling lowers PA contractility.

To clearly define the physiological roles of $Panx1_{EC}$ and $TRPV4_{EC}$ channels, we utilized tamoxifen-inducible, EC-specific $Panx1_{EC}^{-/-}$ and $TRPV4_{EC}^{-/-}$ mice[23, 24]. Tamoxifen-injected $TRPV4^{fl/fl}$ Cre^{-} ($TRPV4^{fl/fl}$) or $Panx1^{fl/fl}$ Cre^{-} ($Panx1^{fl/fl}$) mice were used as controls[8, 23]. $TRPV4_{EC}^{-/-}$ mice showed elevated right ventricular systolic pressure (RVSP), a commonly used *in vivo* indicator of PAP (Fig. 1A). In pressure myography experiments, ATP (1 μmol/L)-induced dilation was absent in PAs from $TRPV4_{EC}^{-/-}$ mice (Fig. 1B), confirming that ATP dilates PAs through $TRPV4_{EC}$ channels. RVSP was also elevated in $Panx1_{EC}^{-/-}$ mice (Fig. 1C). The Fulton Index, a ratio of right ventricular (RV) weight to left ventricle plus septal (LV + S) weight, was not altered in $TRPV4_{EC}^{-/-}$ or $Panx1_{EC}^{-/-}$ mice compared with the respective control mice, suggesting a lack of right ventricular hypertrophy in these mice (Table 1). Importantly, baseline RVSP was not altered in inducible, SMC-specific TRPV4 ($TRPV4_{SMC}^{-/-}$) or Panx1 ($Panx1_{SMC}^{-/-}$) knockout mice (Fig. 1A and C). Functional cardiac MRI studies indicated no alterations in cardiac function in $TRPV4_{EC}^{-/-}$ or $Panx1_{EC}^{-/-}$ mice compared with the respective control mice (Table 1), suggesting that the changes in RVSP were not due to altered cardiac function.

Localized, unitary Ca^{2+} influx signals through $TRPV4_{EC}$ channels, termed *$TRPV4_{EC}$ sparklets*[25], were recorded in *en face*, 4th-order PAs (~ 50 μm) loaded with Fluo-4. Baseline $TRPV4_{EC}$ sparklet activity and activity induced by a low concentration (1 nmol/L) of the specific TRPV4 channel agonist, GSK1016790A (hereafter, GSK101), were significantly reduced in PAs from $Panx1_{EC}^{-/-}$ mice compared with those from $Panx1^{fl/fl}$ mice (Fig. 1D). Additionally, the number of $TRPV4_{EC}$ sparklet sites per cell was decreased in PAs from $Panx1_{EC}^{-/-}$ mice (Fig. 1E). At a

higher level of TRPV4 channel activation (30 nmol/L GSK101), sparklet activity per site and sparklet sites per cell were not different between $Panx1_{EC}^{-/-}$ and control ($Panx1^{fl/fl}$) mice (Fig. 1F). Further, outwards currents through $TRPV4_{EC}$ channels, elicited by 10 nM GSK101, were also lower in $Panx1_{EC}^{-/-}$ than $Panx1^{fl/fl}$ mice (Fig. 1G, *left* and *center*). However, $TRPV4_{EC}$ channel currents, elicited by 100 nM GSK101, were not different between $Panx1_{EC}^{-/-}$ and $Panx1^{fl/fl}$ mice (Fig. 1G, *right*). These data support the concept that the reduced $TRPV4_{EC}$ channel activity in $Panx1_{EC}^{-/-}$ mice is due to impaired channel regulation rather than a decrease in the number of functional $TRPV4_{EC}$ channels. Moreover, isolated, pressurized 4th-order PAs (Fig. 1H) from $TRPV4_{EC}^{-/-}$ mice and $Panx1_{EC}^{-/-}$ mice exhibited a greater contractile response to the thromboxane A_2 receptor agonist U46619 (1–300 nmol/L; Fig. 1I). Together, these data provide the first evidence that $Panx1_{EC}$, via regulation of $TRPV4_{EC}$ channel activity, lowers resting PAP.

$Panx1_{EC}$-generated eATP acts through purinergic $P2Y2R_{EC}$ stimulation to activate $TRPV4_{EC}$ channels.

Bioluminescence measurements confirmed lower baseline eATP levels in PAs from $Panx1_{EC}^{-/-}$ mice compared with PAs from $Panx1^{fl/fl}$ mice (Fig. 2A), supporting an essential role for $Panx1_{EC}$ channels as an eATP-release mechanism in PAs. PAs from $TRPV4_{EC}^{-/-}$ mice, however, exhibited unaltered basal eATP levels. eATP was recently identified as a novel endogenous activator of $TRPV4_{EC}$ channels in the pulmonary circulation[9]. Therefore, we tested whether $Panx1_{EC}$ activates $TRPV4_{EC}$ channels via eATP release. Addition of the eATP-hydrolyzing enzyme apyrase (100 U/mL) reduced the activity of $TRPV4_{EC}$ sparklets in PAs from control mice but not those from $Panx1_{EC}^{-/-}$ mice (Fig. 2B), confirming the role of $Panx1_{EC}$-mediated eATP in $TRPV4_{EC}$ channel activation.

The pulmonary endothelium expresses both P2X and P2Y purinergic receptors[26-29]. The main P2Y receptor subtypes in the pulmonary endothelium are P2Y1R and P2Y2R[13, 26, 29]. The selective P2Y1R inhibitor MRS2179 (MRS, 10 μmol/L) did not alter eATP activation of $TRPV4_{EC}$ sparklets (Fig. 2C). In contrast, the selective P2Y2R inhibitor AR-C 118925XX (AR-C; 10 μmol/L) completely abrogated the effect of eATP on $TRPV4_{EC}$ sparklets (Fig. 2C). eATP was also unable to activate $TRPV4_{EC}$ sparklets in inducible, endothelium-specific $P2Y2R^{-/-}$ ($P2Y2R_{EC}^{-/-}$) mice (Fig. 2C), providing further evidence that eATP activates $TRPV4_{EC}$ channels in PAs specifically via $P2Y2R_{EC}$ signaling. The general P2X1-5 receptor inhibitor, PPADS (10 μmol/L), and P2X7 receptor inhibitor, JNJ-47965567 (JNJ, 1 μmol/L), did not alter the effect of eATP on $TRPV4_{EC}$ sparklets, ruling out a role for P2X1-5/7 receptors in eATP activation of $TRPV4_{EC}$ channels in PAs (Fig. 2D). In ECs freshly isolated from PAs of C57BL6 mice, ATP (10 μM) increased the outward currents through TRPV4 channels (Fig. 2E). Furthermore, the selective P2Y2R agonist, 2-thiouridine-5'-triphosphate (2-thio UTP; 0.5 μmol/L) activated $TRPV4_{EC}$ sparklets in PAs from $P2Y2R^{fl/fl}$ mice but not in PAs from $P2Y2R_{EC}^{-/-}$ mice (Fig. 2F).

Similar to $TRPV4_{EC}^{-/-}$ and $Panx1_{EC}^{-/-}$ mice, $P2Y2R_{EC}^{-/-}$ mice also showed elevated RVSP and an unaltered Fulton Index (Fig. 2G). Taken together, these findings demonstrate that $P2Y2R_{EC}$ is the signaling intermediate for $Panx1_{EC}$–$TRPV4_{EC}$ interactions in PAs.

$Cav\text{-}1_{EC}$ provides a scaffold for $Panx1_{EC}$–$P2Y2R_{EC}$–$TRPV4_{EC}$ signaling.

$Cav\text{-}1_{EC}$, an essential structural protein in the pulmonary circulation[21, 22, 30], has been shown to co-localize with Panx1, P2Y2R, and TRPV4 channels in multiple cell types[17-19, 31]. Therefore, we hypothesized that $Cav\text{-}1_{EC}$ provides a signaling scaffold that supports and maintains the spatial

proximity among the individual elements in the Panx1$_{EC}$–P2Y2R$_{EC}$–TRPV4$_{EC}$ pathway. To clearly delineate the role of Cav-1$_{EC}$ in Panx1$_{EC}$-dependent signaling, we utilized inducible, endothelium-specific Cav-1–knockout mice (Cav-1$_{EC}^{-/-}$; Fig. 3A and B). The loss of Cav-1$_{EC}$ resulted in elevated RVSP in the absence of right ventricular hypertrophy (Fig. 3C), indicating a crucial role of Cav-1$_{EC}$ in maintaining a low resting PAP. Baseline TRPV4$_{EC}$ sparklet activity and activity induced by a low level of GSK101 (1 nmol/L) were reduced in PAs from Cav-1$_{EC}^{-/-}$ mice (Fig. 3D). However, higher-level activation of TRPV4$_{EC}$ channels (30 nmol/L GSK101) resulted in similar TRPV4$_{EC}$ sparklet activity between groups, suggesting that the number of functional TRPV4$_{EC}$ channels is unaltered in Cav-1$_{EC}^{-/-}$ mice (Fig. 3D). Importantly, eATP-induced activation of TRPV4$_{EC}$ sparklets was absent in PAs from Cav-1$_{EC}^{-/-}$ mice (Fig. 3E). These results provided the first functional evidence that Cav-1$_{EC}$ is required for eATP–P2Y2R$_{EC}$–TRPV4$_{EC}$ signaling in PAs. To provide additional evidence to support Cav-1$_{EC}$–dependent co-localization of Panx1$_{EC}$–P2Y2R$_{EC}$–TRPV4$_{EC}$ signaling elements in PAs, we performed *in situ* proximity ligation assays (PLA), which confirmed that Cav-1$_{EC}$ exists within nanometer proximity of Panx1$_{EC}$, P2Y2R$_{EC}$, and TRPV4$_{EC}$ channels in PAs (Fig. 3F).

Cav-1$_{EC}$ anchoring of PKCα mediates P2Y2R$_{EC}$-dependent activation of TRPV4$_{EC}$ channels in PAs.

P2Y2R is a Gq protein-coupled receptor that activates the phospholipase C (PLC)–diacylglycerol (DAG)–PKC signaling pathway. Notably, PKC is known to phosphorylate TRPV4 channels and potentiate its activity[32]. eATP, the DAG analog OAG (1 μmol/L), and the PKC activator phorbol myristate acetate (PMA; 10 nmol/L) stimulated TRPV4$_{EC}$ sparklet activity in

small PAs (Fig. 4A–C). Inhibition of PLC with U73122 (3 μmol/L) abolished eATP activation of $TRPV4_{EC}$ sparklets, but not OAG- or PMA-induced activation of $TRPV4_{EC}$ sparklets. Moreover, the PKCα/β inhibitor Gö-6976 (1 μmol/L) prevented activation of $TRPV4_{EC}$ sparklets by ATP, OAG and PMA (Fig. 4A–C), supporting the concept that eATP activation of $P2Y2R_{EC}$ stimulates $TRPV4_{EC}$ channel activity via PLC–DAG–PKC signaling in PAs. $TRPV4_{EC}$ channel activation by PLC–DAG–PKC signaling was further supported by increased activity of $TRPV4_{EC}$ sparklets in PAs from Cdh5-optoα1 adrenergic receptor (Cdh5-optoα1AR) mouse, which expresses light-sensitive α1AR in endothelial cells. When activated with light (~473 nm), Optoα1AR generates the secondary messengers IP3 and diacylglycerol (DAG)[33]. Light activation resulted in increased activity of $TRPV4_{EC}$ sparklets (Fig. 4D), an effect that was abolished by the PKCα/β inhibitor Gö-6976 (1 μM).

Since Cav-1 possesses a PKC-binding domain[34] and exists in nanometer proximity with $TRPV4_{EC}$ channels and $P2Y2R_{EC}$, we tested the hypothesis that $Cav\text{-}1_{EC}$ anchoring of PKC mediates $P2Y2R_{EC}$–$TRPV4_{EC}$ channel interaction in PAs. PLA experiments confirmed that PKC also exists in nanometer proximity with $Cav\text{-}1_{EC}$ in PAs (Fig. 5A). The PKC-dependence of $Cav\text{-}1_{EC}$ activation of $TRPV4_{EC}$ channels was confirmed by studies in HEK293 cells transfected with TRPV4 alone or TRPV4 channels plus Cav-1 (Fig. 5B), which showed that TRPV4 currents were increased in the presence of Cav-1. Further, the PKCα/β inhibitor Gö-6916 (1 μmol/L) reduced TRPV4 channel currents in Cav-1/TRPV4–co-transfected cells to the level of that in cells transfected with TRPV4 alone (Fig. 5B and C). These results imply that Cav-1 enhances TRPV4 channel activity via PKCα/β anchoring. Experiments in which TRPV4 channels were co-expressed with PKCα or PKCβ showed that only PKCα increased currents through TRPV4 channels (Fig. 5D). Collectively, these results support the conclusion that $Panx1_{EC}$–$P2Y2R_{EC}$–

PKCα–TRPV4$_{EC}$ signaling on a Cav-1$_{EC}$ scaffold reduces PA contractility and lowers resting PAP (Fig. 5E).

Discussion

Regulation of PA contractility and PAP is a complex process involving multiple cell types and signaling elements. In particular, the endothelial signaling mechanisms that control resting PAP remain poorly understood. Our studies identify a Panx1$_{EC}$ and TRPV4$_{EC}$ channel-containing signaling nanodomain that reduces PA contractility and lowers PAP. Although both Panx1$_{EC}$ and TRPV4$_{EC}$ channels have been implicated in dilation of systemic arteries, their impact on PAP remains unknown. We demonstrate critical roles for several key, linked mechanistic, pathways showing that 1) Panx1$_{EC}$ increases eATP levels in small PAs; 2) Panx1$_{EC}$-generated eATP, in turn, enhances Ca^{2+} influx through TRPV4$_{EC}$ channels, thereby dilating PAs and lowering PAP; 3) eATP acts through purinergic P2Y2R$_{EC}$–PKCα signaling to activate TRPV4$_{EC}$ channels; and 4) Cav-1$_{EC}$ provides a signaling scaffold that ensures spatial proximity among the elements of the Panx1$_{EC}$–P2Y2R$_{EC}$–PKCα–TRPV4$_{EC}$ pathway. Our findings reveal a novel signaling axis that can be engaged by physiological stimuli to lower PAP and could also be therapeutically targeted in pulmonary vascular disorders. Moreover, the conclusions in this study may assist in future investigations of the mechanisms underlying pulmonary endothelial dysfunction.

Both ECs and SMCs control vascular contractility and arterial pressure. The expression of Panx1 and TRPV4 channels in both ECs and SMCs[8, 18, 35-37] makes it challenging to decipher the cell type-specific roles of Panx1 and TRPV4 channels using global knockouts or pharmacological strategies. Therefore, studies utilizing EC- or SMC-specific knockout mice are necessary for a

definitive assessment of the control of PAP by EC and SMC Panx1 and TRPV4 channels. Although SMC TRPV4 channels have been shown to contribute to hypoxia-induced pulmonary vasoconstriction, resting PAP is not altered in global TRPV4$^{-/-}$ mice[38, 39]. Further, our studies indicate that SMC Panx1 and TRPV4 channels do not influence resting PAP. Taken together with findings from EC-knockout mice, these results provide strong evidence that endothelial, but not SMC, Panx1 and TRPV4 channels maintain low PA contractility and PAP under basal conditions.

Recent studies in pulmonary fibroblasts and other cell types suggest that TRPV4 channel-mediated increases in cytosolic Ca^{2+} can induce eATP release through Panx1[40, 41]. However, the reverse interaction, in which Panx1-mediated eATP release activates TRPV4 channels, has not been explored in any cell type. Since Panx1 is activated by cytosolic Ca^{2+} [42] and eATP has been previously shown to activate TRPV4$_{EC}$ channels[9], bidirectional signaling between Panx1 and TRPV4 channels is conceivable. However, our demonstration that baseline eATP levels are unchanged in PAs from TRPV4$_{EC}^{-/-}$ mice rules out a role for TRPV4$_{EC}$ channels in controlling eATP release under baseline conditions. Nevertheless, these data from pulmonary ECs do not rule out potential TRPV4–Ca^{2+}–Panx1 signaling in other cell types.

Elevated capillary TRPV4$_{EC}$ channel activity has been linked to increased endothelial permeability[43, 44], lung injury[45], and pulmonary edema[43, 44]. Moreover, Panx1$_{EC}$-mediated eATP release is associated with vascular inflammation at the level of capillaries[8]. The physiological roles of Panx1$_{EC}$ and TRPV4$_{EC}$ channels in PAs, however, remain unknown. ECs from pulmonary capillaries and arteries are structurally and functionally different. Whereas PAs control pulmonary vascular resistance and PAP, capillaries control vascular permeability. TRPV4$_{EC}$ channels couple with distinct targets in arterial and capillary ECs [25, 46]. Our data identify physiological roles of

256 Panx1$_{EC}$–TRPV4$_{EC}$ channel signaling in PAs, but whether such signaling operates in the capillary
257 endothelium and is essential for its physiological function is unclear.

258 Purinergic signaling and the endogenous purinergic receptor agonist eATP are essential
259 controllers of pulmonary vascular function[13, 26, 28, 47]. Our discovery of the Panx1$_{EC}$–P2Y2R$_{EC}$–
260 TRPV4$_{EC}$ pathway establishes a signaling axis in ECs that regulates pulmonary vascular function.
261 The pulmonary vasculature is a high-flow circulation, and pulmonary ECs have been shown to
262 release eATP in response to flow/shear stress[12]. Therefore, flow/shear stress could be a potential
263 physiological activator of Panx1$_{EC}$–P2Y2R$_{EC}$–TRPV4$_{EC}$ signaling in PAs. Further studies are
264 needed to verify this possibility. Several purinergic receptor subtypes are expressed in the
265 pulmonary vasculature, including P2YRs and P2XRs[26-28]. Although only P2Y2R$_{EC}$ appears to
266 mediate eATP activation of TRPV4$_{EC}$ channels, our studies do not rule out potentially important
267 roles for other P2Y or P2X receptors in the pulmonary endothelium.

268 Activation of TRPV4$_{EC}$ channels by eATP released through Panx1$_{EC}$ in PAs would be
269 facilitated by spatial localization of TRPV4$_{EC}$ channels with Panx1$_{EC}$. In keeping with this, several
270 scaffolding proteins are known to promote localization of TRPV4 channels with their regulatory
271 proteins, including A-kinase anchoring protein 150 (AKAP150) and Cav-1[23, 48]. Although
272 AKAP150 is not found in the pulmonary endothelium[9], Cav-1 is a key structural protein in the
273 pulmonary vasculature and has a well-established role in controlling pulmonary vascular function,
274 as demonstrated by increased RVSP in global Cav-1$^{-/-}$ mice[49, 50]. Moreover, Cav-1–dependent
275 signaling is impaired in pulmonary hypertension[20-22]. Studies in other cell types have shown that
276 Cav-1 can co-localize with Panx1 and P2Y2Rs[18, 19]. Additionally, Cav-1 can interact with PKC at
277 the Cav-1 scaffolding domain[34]. Our results demonstrate that Cav-1$_{EC}$ exists in nanometer
278 proximity with Panx1$_{EC}$, P2Y2R$_{EC}$, PKC, and TRPV4$_{EC}$ channels in PAs. Furthermore, the

activation of $TRPV4_{EC}$ channels by $Panx1_{EC}$, eATP, $P2Y2R_{EC}$ or PKCα requires $Cav\text{-}1_{EC}$. Based on these findings, we conclude that $Cav\text{-}1_{EC}$ enables $Panx1_{EC}$–$P2Y2R_{EC}$–$TRPV4_{EC}$ signaling at EC membranes in PAs. Cav-1 is also a well-known anchor protein for eNOS[16], acting by stabilizing eNOS expression and negatively regulating its activity[16]. We previously showed that $TRPV4_{EC}$ Ca^{2+} sparklets activate eNOS in PAs[9, 36]. Thus, $Cav\text{-}1_{EC}$ enhancement of Ca^{2+} influx through $TRPV4_{EC}$ channels may represent novel mechanisms for regulating eNOS activity.

$Cav\text{-}1_{EC}$/PKCα-dependent signaling is a novel endogenous mechanism for activating arterial $TRPV4_{EC}$ channels and lowering PAP. Proximity to PKCα appears to be crucial for the normal function of TRPV4 channels. Evidence from the systemic circulation suggests that co-localization of TRPV4 channels with scaffolding proteins enhances their activity[51, 52], and we specifically demonstrated that PKC anchoring by AKAP150 enhances the activity of $TRPV4_{EC}$ channels in mesenteric arteries[23]. Here, we show that PKC anchoring by $Cav\text{-}1_{EC}$ enables PKC activation of $TRPV4_{EC}$ channels in PAs. This discovery raises the possibility that disruption of PKC anchoring by $Cav\text{-}1_{EC}$ could impair the $Panx1_{EC}$–$P2Y2R_{EC}$–$TRPV4_{EC}$ signaling axis under disease conditions. A lack of PKC anchoring by scaffolding proteins in systemic arteries has been demonstrated in obesity and hypertension[23, 52]. Further studies of pulmonary vascular disorders are required to establish whether the $Panx1_{EC}$–$P2Y2R_{EC}$–PKCα–$TRPV4_{EC}$ signaling axis is impaired in pulmonary vascular disorders.

In conclusion, $Panx1_{EC}$–$TRPV4_{EC}$ signaling reduces PA contractility and maintains a low resting PAP. This mechanism is facilitated by eATP released through $Panx1_{EC}$ and subsequent activation of $P2Y2R_{EC}$–PKCα signaling. $Cav\text{-}1_{EC}$ ensures the spatial proximity among $Panx1_{EC}$, $P2Y2R_{EC}$, and $TRPV4_{EC}$ channels and also anchors PKCα close to $TRPV4_{EC}$ channels. These findings identify a novel endothelial Ca^{2+} signaling mechanism that reduces PA contractility.

Further investigations are needed to determine whether impairment of this pathway contributes to elevated PAP in pulmonary vascular disorders and whether this pathway can be targeted for therapeutic benefit.

Materials and Methods

Drugs and chemical compounds.

Cyclopiazonic acid (CPA), GSK2193874, GSK1016790A, Phorbol 12-myristate 13-acetate (PMA), AR-C 118925XX, 2-Thio UTP tetrasodium salt, MRS2179, U-73122 and NS309 were purchased from Tocris Bioscience (Minneapolis, MN, USA). Fluo-4-AM (Ca^{2+} indicator) were purchased from Invitrogen (Carlsbad, CA, USA). 1-O-9Z-octadecenoyl-2-O-acetyl-*sn*-glycerol (OAG), PPADS (sodium salt), Gö-6976, JNJ-47965567 and U46619 were purchased from Cayman Chemicals (Ann Arbor, MI, USA). Tamoxifen and apyrase were obtained from Sigma-Aldrich（St. Louis, MO, USA).

Animal protocols and models.

All animal protocols were approved by the University of Virginia Animal Care and Use Committee (protocols 4100 and 4120). This study was performed in strict accordance with the recommendations in the Guide for the Care and Use of Laboratory Animals of the National Institutes of Health. For surgical procedures, every effort was made to minimize suffering. Both male and female mice were used in this study and age- and sex-matched controls were used. C57BL6/J were obtained from the Jackson Laboratory (Bar Harbor, ME). Inducible endothelial

cell (EC)-specific TRPV4 channel knockout ($TRPV4_{EC}^{-/-}$)[53, 54], smooth muscle cell (SMC)-specific TRPV4 channel knockout ($TRPV4_{SMC}^{-/-}$)[55], EC caveolin-1 knockout ($Cav\text{-}1_{EC}^{-/-}$)[56], EC-specific P2Y2R receptor knockout ($P2Y2R_{EC}^{-/-}$)[57], EC-specific Panx1 channel knockout ($Panx1_{EC}^{-/-}$)[24, 54] and SMC-specific Panx1 channel knockout ($Panx1_{SMC}^{-/-}$)[55] mice (10-14 weeks old) were used. The mouse strain Cdh5-optoα1AR was developed by CHROMus™ which is supported by the National Heart Lung Blood Institute of the National Institute of Health under award number R24HL120847. Mice were housed in an enriched environment and maintained under a 12:12 h light/dark photocycle at ~23°C with fresh tap water and standard chow diet available *ad libitum.* Mice were euthanized with pentobarbital (90 mg/kg^{-1}; intraperitoneally; Diamondback Drugs, Scottsdale, AZ) followed by cervical dislocation for harvesting lung tissue. Fourth-order pulmonary arteries (PAs, ~50 μm diameter) were isolated in cold HEPES-buffered physiological salt solution (HEPES-PSS, in mmol/L, 10 HEPES, 134 NaCl, 6 KCl, 1 $MgCl_2$ hexahydrate, 2 $CaCl_2$ dihydrate, and 7 dextrose, pH adjusted to 7.4 using 1 mol/L NaOH).

$TRPV4^{fl/fl}$ [53], $Cav\text{-}1^{fl/fl}$ [56], $Panx1^{fl/fl}$ [24, 54] and $P2Y2R^{fl/fl}$ [57]mice were crossed with VE-Cadherin (Cdh5, endothelial) Cre mice[53] or SMMHC (smooth muscle) Cre mice [58]. EC- or SMC-specific knockout of TRPV4, Cav-1, Panx1, or P2Y2R was induced by injecting 6 week-old $TRPV4^{fl/fl}$ Cre^{+}, $Cav\text{-}1^{fl/fl}$ Cre^{+}, $Panx1^{fl/fl}$ Cre^{+} and $P2Y2R^{fl/fl}$ Cre^{+} mice with tamoxifen (40 mg/kg intraperitoneally per day for 10 days). Tamoxifen-injected $TRPV4^{fl/fl}$ Cre^{-}, $Cav\text{-}1^{fl/fl}$ Cre^{-}, $Panx1^{fl/fl}$ Cre^{-} and $P2Y2R^{fl/fl}$ Cre^{-} mice were used as controls. Mice were used for experiments after a two-week washout period. Genotypes for Cdh5 Cre and SMMHC Cre were confirmed following previously published protocols[53, 58]. $TRPV4^{fl/fl}$[53], $Cav\text{-}1^{fl/fl}$[56], $Panx1^{fl/fl}$[24, 54], $P2Y2R^{fl/fl}$[57] genotyping was performed as described previously. Cdh5-Optoα1AR mice were developed by CHROMus (Cornell University, USA).

346

347 **Right ventricular systolic pressure (RVSP) and Fulton Index measurement.**

348 Mice were anesthetized with pentobarbital (50 mg/kg bodyweight; intraperitoneally) and
349 bupivacaine HCl (100 μL of 0.25% solution; subcutaneously) was used to numb the dissection site
350 on the mouse. RVSP was measured as an indirect indicator of pulmonary arterial pressure (PAP).
351 A Mikro-Tip pressure catheter (SPR-671; Millar Instruments, Huston, TX), connected to a bridge
352 amp (FE221), and a PowerLab 4/35 4-channel recorder (Instruments, Colorado Springs, CO), was
353 cannulated through the external jugular vein into the right ventricle. Right ventricular pressure and
354 heart rate were acquired and analyzed using LabChart8 software (ADInstruments, Colorado
355 Springs, CO). A stable 3-minute recording was acquired for all the animals, and 1-minute
356 continuous segment was used for data analysis. When necessary, traces were digitally filtered
357 using a low-pass filter at a cut-off frequency of 50 Hz. At the end of the experiments, mice were
358 euthanized, and the hearts were isolated for right ventricular hypertrophy analysis. Right
359 ventricular hypertrophy was determined by calculating the Fulton Index, a ratio of the right
360 ventricular (RV) heart weight over the left ventricular (LV) plus septum (S) weight (RV/ LV+S).

361

362 **Luciferase assay for total ATP release.**

363 ATP assay protocol was adapted from Yang et al.[59]. Fourth-order pulmonary arteries
364 (PAs, ~ 50 μm diameter) were isolated in cold HEPES-buffered physiological salt
365 solution (HEPES-PSS, in mmol/L, 10 HEPES, 134 NaCl, 6 KCl, 1 $MgCl_2$ hexahydrate, 2
366 $CaCl_2$ dihydrate, and 7 dextrose, pH adjusted to 7.4 using 1 mol/L NaOH). Isolated PAs were
367 pinned down *en face* on a Sylgard block and cut open. PAs were placed in black, opaque 96-well

plates and incubated in HEPES-PSS for 10 minutes at 37 °C, followed by incubation with the ectonucleotidase inhibitor ARL 67156 (300 μmol/L, Tocris Bioscience, Minneapolis, MN) for 30 minutes at 37 °C. 50 μL volume of each sample was transferred to another black, opaque 96-well plate. ATP was measured using ATP bioluminescence assay reagent ATP Bioluminescence HSII kit (Roche Applied Science, Penzberg, Germany). Using a luminometer (FluoStar Omega), 50 μL of luciferin:luciferase reagent (ATP bioluminescence assay kit HSII; Roche Applied Science, Penzberg, Germany) was injected into each well and luminescence was recorded following a 5 second orbital mix and sample measurement at 7 seconds. ATP concentration in each sample was calculated from an ATP standard curve.

Cardiac Magnetic Resonance Imaging (MRI).

MRI studies were conducted under protocols that comply with the Guide for the Care and Use of Laboratory Animals (NIH publication no. 85-23, Revised 1996). Mice were positioned in the scanner under 1.25% isoflurane anesthesia and body temperature was maintained at 37°C using thermostatic circulating water. A cylindrical birdcage RF coil (30 mm-diameter, Bruker, Ettlingen, Germany) with an active length of 70 mm was used, and heart rate, respiration, and temperature were monitored during imaging using a fiber optic, MR-compatible system (Small Animal Imaging Inc., Stony Brook, NY). MRI was performed on a 7 Tesla (T) Clinscan system (Bruker, Ettlingen, Germany) equipped with actively shielded gradients with a full strength of 650 mT/m and a slew rate of 6666 mT/m/ms[60]. Six short-axis slices were acquired from base to apex, with slice thickness of 1 mm, in-plane spatial resolution of 0.2 × 0.2 mm^2, and temporal resolution of 8–12 ms. Baseline ejection fraction (EF), end-diastolic volume (EDV), end-systolic volume

(ESV), myocardial mass, wall thickness, stroke volume (SV), and cardiac output (CO) were assessed from the cine images using the freely available software Segment version 2.0 R5292 (http://segment.heiberg.se).

Pressure myography.

Isolated mouse PAs (~ 50 μm) were cannulated on glass micropipettes in a pressure myography chamber (The Instrumentation and Model Facility, University of Vermont, Burlington, VT) at areas lacking branching points, and were pressurized at a physiological pressure of 15 mm Hg[36]. Arteries were superfused with PSS (in mmol/L, 119 NaCl, 4.7 KCl, 1.2 KH_2PO_4, 1.2 $MgCl_2$ hexahydrate, 2.5 $CaCl_2$ dihydrate, 7 dextrose, and 24 $NaHCO_3$) at 37°C and bubbled with 20% O_2/5% CO_2 to maintain the pH at 7.4. All drug treatments were added to the superfusing PSS. PAs were pre-constricted with 50 nmol/L U46619 (a thromboxane A2 receptor agonist). All other pharmacological treatments were performed in the presence of U46619. Before measurement of vascular reactivity, arteries were treated with NS309 (1 μmol/L), a direct opener of endothelial IK/SK channels, to assess endothelial health. Arteries that failed to fully dilate to NS309 were discarded. Changes in arterial diameter were recorded at a 60-ms frame rate using a charge-coupled device camera and edge-detection software (IonOptix LLC, Westwood, MA) [25, 52]. All drug treatments were incubated for 10 minutes. At the end of each experiment, Ca^{2+}-free PSS (in mmol/L, 119 NaCl, 4.7 KCl, 1.2 KH_2PO_4, 1.2 $MgCl_2$ hexahydrate, 7 dextrose, 24 $NaHCO_3$, and 5 EGTA) was applied to assess the maximum passive diameter. Percent constriction was calculated by:

412 $[(Diameter_{before} - Diameter_{after})/Diameter_{before}] \times 100$ (1)

413

414 where $Diameter_{before}$ is the diameter of the artery before a treatment and $Diameter_{after}$ is the

415 diameter after the treatment. Percent dilation was calculated by:

416

417 $[(Diameter_{dilated} - Diameter_{basal})/(Diameter_{Ca-free} - Diameter_{basal})] \times 100$ (2)

418

419 where $Diameter_{basal}$ is the stable diameter before drug treatment, $Diameter_{dilated}$ is the diameter after

420 drug treatment, and $Diameter_{Ca\text{-}free}$ is the maximum passive diameter.

421

422 **Ca^{2+} imaging.**

423 Measurements of $TRPV4_{EC}$ Ca^{2+} sparklets in the native endothelium of mouse PAs were

424 performed as previously described[25]. Briefly, 4th-order (~ 50 μm) PAs were pinned down *en face*

425 on a Sylgard block and loaded with fluo-4-AM (10 μmol/L) in the presence of pluronic acid

426 (0.04%) at 30°C for 30 minutes. $TRPV4_{EC}$ Ca^{2+} sparklets were recorded at 30 frames per second

427 with Andor Revolution WD (with Borealis) spinning-disk confocal imaging system (Oxford

428 Instruments, Abingdon, UK) comprised of an upright Nikon microscope with a 60X water dipping

429 objective (numerical aperture 1.0) and an electron multiplying charge coupled device camera

430 (iXon 888, Oxford Instruments, Abingdon, UK). All experiments were carried out in the presence

431 of cyclopiazonic acid (20 μmol/L, a sarco-endoplasmic reticulum (ER) Ca^{2+}-ATPase inhibitor)

in order to eliminate the interference from Ca^{2+} release from intracellular stores. Fluo-4 was excited at 488 nm with a solid-state laser and emitted fluorescence was captured using a 525/36-nm band-pass filter. $TRPV4_{EC}$ Ca^{2+} sparklets were recorded before and 5 minutes after the addition of specific compounds. To generate fractional fluorescence (F/F_0) traces, a region of interest defined by a 1.7-μm^2 (5×5 pixels) box was placed at a point corresponding to peak sparklet amplitude. Each field of view was ~ 110×110 μm and covered ~ 15 ECs. Representative F/F_0 traces were filtered using a Gaussian filter and a cutoff corner frequency of 4 Hz. Sparklet activity was assessed as described previously using the custom-designed SparkAn software [25, 52].

For the experiments in Cdh5-optoα1AR mice, PAs were loaded with X-Rhod-1 AM (5 μM, Thermo Fisher Scientific Inc., Waltham, MA, USA) for 30 minutes at 30°C. X-Rhod-1 was excited at 561 nm and the emitted light was captured with a 607/36-nm band-pass filter. Optoα1AR was activated at 470 nm for 5 seconds using pE-4000 (CoolLED Ltd, Andover, UK).

Calculation of TRPV4 sparklet activity per site.

Activity of TRPV4 Ca^{2+} sparklets was evaluated as described previously[25, 52]. Area under the curve for all the events at a site was determined using trapezoidal numerical integration ($[F-F_0]/F_0$ over time, in seconds). The average number of active TRPV4 channels, as defined by NP_O (where N is the number of channels at a site and P_O is the open state probability of the channel), was calculated by

$$NP_O = (T_{level1} + 2T_{level2} + 3T_{level3} + 4T_{level4}) / T_{total} \quad (3)$$

where T is the dwell time at each quantal level detected at TRPV4 sparklet sites and T_{total} is the duration of the recording. NP_O was determined using Single Channel Search module of Clampfit and quantal amplitudes derived from all-points histograms [9] ($\Delta F/F_0$ of 0.29 for Fluo-4 –loaded PAs).

Total number of sparklet sites in a field was divided by the number of cells in that field to obtain sparklet sites per cell.

Immunostaining.

Immunostaining was performed on 4th-order PAs (~ 50 μm) pinned *en face* on SYLGARD blocks. PAs were fixed with 4% paraformaldehyde (PFA) at room temperature for 15 minutes and then washed 3 times with phosphate-buffered saline (PBS). The tissue was permeabilized with 0.2% Triton-X for 30 minutes, blocked with 5% normal donkey serum (ab7475, Abcam, Cambridge, MA) or normal goat serum (ab7475, Abcam, Cambridge, MA), depending on the host of the secondary antibody used, for 1 hour at room temperature. PAs were incubated with the primary antibodies (Table 2) overnight at 4°C. Following the overnight incubation, PAs were incubated with secondary antibody 1:500 Alexa Fluor® 568-conjugated donkey anti-rabbit (Life Technologies, Carlsbad, CA, USA) for one hour at room temperature in the dark room. For nuclear staining, PAs were washed with PBS and then incubated with 0.3 mmol/L DAPI (Invitrogen, Carlsbad, CA, USA) for 10 minutes at room temperature. Images were acquired along the z-axis from the surface of the endothelium to the bottom where the EC layer encounters the smooth muscle cell layer with a slice size of 0.1 μm using the Andor microscope described above. The

internal elastic lamina (IEL) autofluorescence was evaluated using an excitation of 488 nm with a solid-state laser and collecting the emitted fluorescence with a 525/36 nm band-pass filter. Immunostaining for the protein of interest was evaluated using an excitation of 561 nm and collecting the emitted fluorescence with a 607/36 nm band-pass filter. DAPI immunostaining was evaluated using an excitation of 409 nm and collecting the emitted fluorescence with a 447/69 nm band-pass filter.

In situ Proximity Ligation Assay (PLA).

Fourth-order (~ 50 μm) PAs were pinned *en face* on SYLGARD blocks. PAs were fixed with 4% PFA for 15 minutes followed by three washes with PBS. PAs were then permeabilized with 0.2% Triton X for 30 minutes at room temperature followed by blocking with 5% normal donkey serum (Abcam plc, Cambridge, MA, USA) and 300 mmol/L glycine for one hour at room temperature. After three washes with PBS, PAs were incubated with the primary antibodies (Table 2) overnight at 4 °C. The PLA protocol from Duolink PLA Technology kit (Sigma-Aldrich, St. Louis, MO, USA) was followed for the detection of co-localized proteins. Lastly, PAs were incubated with 0.3 mmol/L DAPI nuclear staining (Invitrogen, Carlsbad, CA, USA) for 10 minutes at room temperature in the dark room. PLA images were acquired using the Andor Revolution spinning-disk confocal imaging system along the z-axis at a slice size of 0.1 μm. Images were analyzed by normalizing the number of positive puncta by the number of nuclei in a field of view.

497 **Table 2. List of antibodies used for immunostaining and PLA on *en face* PAs.**

Protein	Product no.	Company	Clonality	Concentration
TRPV4	LSC 94498	LifeSpan BioScience INC	Polyclonal	1:200
Cav-1	Ab2910	Abcam plc.	Polyclonal	1:500
Cav-1 (PLA only)	NB100-615	Novus Biologicals, LLC	Monoclonal	1:200
PKC	SC-17769	Santa Cruz Biotechnology, Inc.	Monoclonal	1:250
Panx1	ACC-234	Alomone Labs,	Polyclonal	1:100
P2Y2R	APR-010	Alomone Labs,	Polyclonal	1:250
CD-31	RM5201	Invitrogen, Carlsbad, Ca, USA	Monoclonal	1:100

498

499 **Plasmid generation and transfection into HEK293 cells.**

500 The TRPV4 coding sequence without stop codons was amplified from mouse heart cDNA. The

501 amplified fragment was inserted into a plasmid backbone containing a CMV promoter region for

expression and in addition, is suitable for lentiviral production by Gibson assembly. The in-frame FLAG tag was inserted into the 3'-primer used for amplification. Constructs were verified by sequencing the regions that had been inserted into the plasmid backbone. HEK293 cells were seeded (7 x 10^5 cells per 100 mm dish) in Dulbecco's Modified Eagle Medium with 10% fetal bovine serum (Thermo Fisher Scientific Inc., Waltham, MA, USA) 1 day prior to transfection. Cells were transfected using the LipofectamineLTX protocol (Thermo Fisher Scientific Inc., Waltham, MA, USA). TRPV4 was co-expressed with PKCα and PKCβ, obtained from Origene Technologies (Montgomery County, MD).

Patch clamp in HEK293 cells and freshly isolated ECs.

TRPV4 channel current was recorded in HEK293 cells using whole-cell patch configuration 48 hrs after transfection. The intracellular solution consisted of (in mmol/L) 20 CsCl, 100 Cs-aspartate, 1 $MgCl_2$, 4 ATP, 0.08 $CaCl_2$, 10 BAPTA, 10 HEPES, pH 7.2 (adjusted with CsOH). Currents were measured using a voltage clamp protocol where voltage-ramp pulses (-100 mV to +100 mV) were applied over 200 ms with a holding potential of -50 mV. TRPV4 currents were measured before or 5 minutes after treatment. The extracellular solution consisted of (in mmol/L) 10 HEPES, 134 NaCl, 6 KCl, 2 $CaCl_2$, 10 glucose, and 1 $MgCl_2$ (adjusted to pH 7.4 with NaOH). Narishige PC-100 puller (Narishige International USA, INC., Amityville, NY, USA) was utilized to pull patch electrodes using borosilicate glass (O.D.: 1.5 mm; I.D.: 1.17 mm; Sutter Instruments, Novato, CA, USA). Patch electrodes were polished using MicroForge MF-830 polisher (Narishige International USA, INC., Amityville, NY, USA). The pipette resistance was (3–5 ΩM). Amphotericin B was dissolved in the intracellular pipette solution to reach a final concentration of 0.3 μmol/L. Data were acquired using HEKA EPC 10 amplifier and PatchMaster

v2X90 program (Harvard Bioscience, Holliston, MA, USA), and analyzed using FitMaster v2X73.2 (Harvard Bioscience, Holliston, MA, USA) and MATLAB R2018a (MathWorks, Natick, MA, USA).

Fresh ECs were obtained via enzymatic digestion of 4th-order PAs. Briefly, PAs were incubated in the dissociation solution (in mmol/L, 55 NaCl, 80 Na glutamate, 6 KCl, 2 $MgCl_2$, 0.1 $CaCl_2$, 10 glucose, 10 HEPES, pH 7.3) containing Worthington neutral protease (0.5 mg/mL) for 30 minutes at 37°C. The extracellular solution consisted of (in mmol/L) 10 HEPES, 134 NaCl, 6 KCl, 2 $CaCl_2$, 10 glucose, and 1 $MgCl_2$ (adjusted to pH 7.4 with NaOH). The intracellular pipette solution for perforated-patch configuration consisted of (in mmol/L) 10 HEPES, 30 KCl, 10 NaCl, 110 K-aspartate, and 1 $MgCl_2$ (adjusted to pH 7.2 with NaOH). Cells were kept at room temperature in a bathing solution consisting of (in mmol/L) 10 HEPES, 134 NaCl, 6 KCl, 2 $CaCl_2$, 10 glucose, and 1 $MgCl_2$ (adjusted to pH 7.4 with NaOH). TRPV4 channel current was recorded from freshly isolated ECs as described previously [25, 61]. Briefly, GSK101-induced outward currents through TRPV4 channels were assessed in response to a 200-ms voltage step from -45 mV to +100 mV in the presence of ruthenium red in order to prevent Ca^{2+} and activation of IK/SK channels at negative voltages. Outward currents were obtained by averaging the currents through the voltage step. GSK219-sensitive currents were obtained by subtracting the currents in the presence of GSK219 from the currents in the presence of GSK101.

Statistical analysis.

Results are presented as mean ± SEM. The n=1 was defined as one artery in the imaging experiments (Ca^{2+} imaging, PLA), one cell for patch clamp experiments, one mouse for RVSP

548 measurements, one artery for pressure myography experiments, one mouse for functional MRI,
549 one mouse for ATP measurements, and one mouse for qPCR experiments. The data were obtained
550 from at least five mice in experiments performed in at least two independent batches. The
551 individual data points are shown each dataset. For *in vivo* experiments, an independent team
552 member performed random assignment of animals to groups and did not have knowledge of
553 treatment assignment groups. All the *in vivo* experiments were blinded; information about the
554 groups or treatments was withheld from the experimenter or from the team member who analyzed
555 the data.

556 All data are shown in graphical form using CorelDraw Graphics Suite X7 (Ottawa, ON,
557 Canada) and statistically analyzed using GraphPad Prism 8.3.0 (Sand Diego, CA). A power
558 analysis to determine group sizes and study power (>0.8) was performed using GLIMMPSE
559 software ($\alpha = 0.05$; >20% change). Using this method, we estimated at least 5 cells per group for
560 patch clamp experiments, 5 arteries per group for imaging and pressure myography experiments,
561 and 4 mice per group for RVSP measurements and MRI. A Shapiro-Wilk test was performed to
562 determine normality. The data in this article were normally distributed; therefore, parametric
563 statistics were performed. Data were analyzed using two-tailed, paired or independent t-test (for
564 comparison of data collected from two different treatments), one-way ANOVA or two-way
565 ANOVA (to investigate statistical differences among more than two different treatments). Tukey
566 correction was performed for multiple comparisons with one-way ANOVA, and Bonferroni
567 correction was performed for multiple comparisons with two-way ANOVA. Statistical
568 significance was determined as a P value less than 0.05.

569

570

Acknowledgements

The mouse strain cdh5-optoα1AR was developed by CHROMus™ which is supported by the National Heart Lung Blood Institute of the National Institute of Health under award number R24HL120847.

Sources of Funding

This work was supported by grants from the National Institutes of Health to SKS (R01HL142808, R01HL146914) and to VEL/SKS (R01HL157407).

Disclosures

The authors have no conflicts to disclose.

References

1. Navis KE, Fan CY, Trang T, Thompson RJ and Derksen DJ. Pannexin 1 Channels as a Therapeutic Target: Structure, Inhibition, and Outlook. *ACS Chem Neurosci*. 2020;11:2163-2172.
2. Begandt D, Good ME, Keller AS, DeLalio LJ, Rowley C, Isakson BE and Figueroa XF. Pannexin channel and connexin hemichannel expression in vascular function and inflammation. *BMC Cell Biol*. 2017;18:2.
3. Good ME, Begandt D, DeLalio LJ, Keller AS, Billaud M and Isakson BE. Emerging concepts regarding pannexin 1 in the vasculature. *Biochem Soc Trans*. 2015;43:495-501.
4. Bao L, Locovei S and Dahl G. Pannexin membrane channels are mechanosensitive conduits for ATP. *FEBS Lett*. 2004;572:65-8.
5. Lohman AW, Billaud M and Isakson BE. Mechanisms of ATP release and signalling in the blood vessel wall. *Cardiovasc Res*. 2012;95:269-80.
6. Gaynullina D, Shestopalov VI, Panchin Y and Tarasova OS. Pannexin 1 facilitates arterial relaxation via an endothelium-derived hyperpolarization mechanism. *FEBS Lett*. 2015;589:1164-70.
7. Gaynullina D, Tarasova OS, Kiryukhina OO, Shestopalov VI and Panchin Y. Endothelial function is impaired in conduit arteries of pannexin1 knockout mice. *Biol Direct*. 2014;9:8.

8. Sharma AK, Charles EJ, Zhao Y, Narahari AK, Baderdinni PK, Good ME, Lorenz UM, Kron IL, Bayliss DA, Ravichandran KS, Isakson BE and Laubach VE. Pannexin-1 channels on endothelial cells mediate vascular inflammation during lung ischemia-reperfusion injury. *Am J Physiol Lung Cell Mol Physiol*. 2018;315:L301-L312.
9. Marziano C, Hong K, Cope EL, Kotlikoff MI, Isakson BE and Sonkusare SK. Nitric Oxide-Dependent Feedback Loop Regulates Transient Receptor Potential Vanilloid 4 (TRPV4) Channel Cooperativity and Endothelial Function in Small Pulmonary Arteries. *J Am Heart Assoc*. 2017;6.
10. Lyubchenko T, Woodward H, Veo KD, Burns N, Nijmeh H, Liubchenko GA, Stenmark KR and Gerasimovskaya EV. P2Y1 and P2Y13 purinergic receptors mediate Ca2+ signaling and proliferative responses in pulmonary artery vasa vasorum endothelial cells. *Am J Physiol Cell Physiol*. 2011;300:C266-75.
11. McMillan MR, Burnstock G and Haworth SG. Vasodilatation of intrapulmonary arteries to P2-receptor nucleotides in normal and pulmonary hypertensive newborn piglets. *Br J Pharmacol*. 1999;128:543-8.
12. Yamamoto K, Sokabe T, Ohura N, Nakatsuka H, Kamiya A and Ando J. Endogenously released ATP mediates shear stress-induced Ca2+ influx into pulmonary artery endothelial cells. *Am J Physiol Heart Circ Physiol*. 2003;285:H793-803.
13. Konduri GG and Mital S. Adenosine and ATP cause nitric oxide-dependent pulmonary vasodilation in fetal lambs. *Biol Neonate*. 2000;78:220-9.
14. Mamenko M, Zaika O, Jin M, O'Neil RG and Pochynyuk O. Purinergic activation of Ca2+-permeable TRPV4 channels is essential for mechano-sensitivity in the aldosterone-sensitive distal nephron. *PLoS One*. 2011;6:e22824.
15. Lorenzo IM, Liedtke W, Sanderson MJ and Valverde MA. TRPV4 channel participates in receptor-operated calcium entry and ciliary beat frequency regulation in mouse airway epithelial cells. *Proc Natl Acad Sci U S A*. 2008;105:12611-6.
16. Bernatchez PN, Bauer PM, Yu J, Prendergast JS, He P and Sessa WC. Dissecting the molecular control of endothelial NO synthase by caveolin-1 using cell-permeable peptides. *Proc Natl Acad Sci U S A*. 2005;102:761-6.
17. Goedicke-Fritz S, Kaistha A, Kacik M, Markert S, Hofmeister A, Busch C, Banfer S, Jacob R, Grgic I and Hoyer J. Evidence for functional and dynamic microcompartmentation of Cav-1/TRPV4/K(Ca) in caveolae of endothelial cells. *Eur J Cell Biol*. 2015;94:391-400.
18. DeLalio LJ, Keller AS, Chen J, Boyce AKJ, Artamonov MV, Askew-Page HR, Keller TCSt, Johnstone SR, Weaver RB, Good ME, Murphy SA, Best AK, Mintz EL, Penuela S, Greenwood IA, Machado RF, Somlyo AV, Swayne LA, Minshall RD and Isakson BE. Interaction Between Pannexin 1 and Caveolin-1 in Smooth Muscle Can Regulate Blood Pressure. *Arterioscler Thromb Vasc Biol*. 2018;38:2065-2078.
19. Martinez NA, Ayala AM, Martinez M, Martinez-Rivera FJ, Miranda JD and Silva WI. Caveolin-1 Regulates the P2Y2 Receptor Signaling in Human 1321N1 Astrocytoma Cells. *J Biol Chem*. 2016;291:12208-22.
20. Bakhshi FR, Mao M, Shajahan AN, Piegeler T, Chen Z, Chernaya O, Sharma T, Elliott WM, Szulcek R, Bogaard HJ, Comhair S, Erzurum S, van Nieuw Amerongen GP, Bonini MG and Minshall RD. Nitrosation-dependent caveolin 1 phosphorylation, ubiquitination, and degradation and its association with idiopathic pulmonary arterial hypertension. *Pulm Circ*. 2013;3:816-30.
21. Maniatis NA, Shinin V, Schraufnagel DE, Okada S, Vogel SM, Malik AB and Minshall RD. Increased pulmonary vascular resistance and defective pulmonary artery filling in caveolin-1-/- mice. *Am J Physiol Lung Cell Mol Physiol*. 2008;294:L865-73.
22. Nickel NP, Spiekerkoetter E, Gu M, Li CG, Li H, Kaschwich M, Diebold I, Hennigs JK, Kim KY, Miyagawa K, Wang L, Cao A, Sa S, Jiang X, Stockstill RW, Nicolls MR, Zamanian RT, Bland RD and

Rabinovitch M. Elafin Reverses Pulmonary Hypertension via Caveolin-1-Dependent Bone Morphogenetic Protein Signaling. *Am J Respir Crit Care Med*. 2015;191:1273-86.

23. Ottolini M, Hong K, Cope EL, Daneva Z, DeLalio LJ, Sokolowski JD, Marziano C, Nguyen NY, Altschmied J, Haendeler J, Johnstone SR, Kalani MY, Park MS, Patel RP, Liedtke W, Isakson BE and Sonkusare SK. Local Peroxynitrite Impairs Endothelial TRPV4 Channels and Elevates Blood Pressure in Obesity. *Circulation*. 2020.

24. Poon IK, Chiu YH, Armstrong AJ, Kinchen JM, Juncadella IJ, Bayliss DA and Ravichandran KS. Unexpected link between an antibiotic, pannexin channels and apoptosis. *Nature*. 2014;507:329-34.

25. Sonkusare SK, Bonev AD, Ledoux J, Liedtke W, Kotlikoff MI, Heppner TJ, Hill-Eubanks DC and Nelson MT. Elementary Ca2+ signals through endothelial TRPV4 channels regulate vascular function. *Science*. 2012;336:597-601.

26. Konduri GG, Bakhutashvili I, Frenn R, Chandrasekhar I, Jacobs ER and Khanna AK. P2Y purine receptor responses and expression in the pulmonary circulation of juvenile rabbits. *Am J Physiol Heart Circ Physiol*. 2004;287:H157-64.

27. Syed NI, Tengah A, Paul A and Kennedy C. Characterisation of P2X receptors expressed in rat pulmonary arteries. *European journal of pharmacology*. 2010;649:342-8.

28. Hennigs JK, Luneburg N, Stage A, Schmitz M, Korbelin J, Harbaum L, Matuszcak C, Mienert J, Bokemeyer C, Boger RH, Kiefmann R and Klose H. The P2-receptor-mediated Ca(2+) signalosome of the human pulmonary endothelium - implications for pulmonary arterial hypertension. *Purinergic Signal*. 2019;15:299-311.

29. Zemskov E, Lucas R, Verin AD and Umapathy NS. P2Y receptors as regulators of lung endothelial barrier integrity. *Journal of cardiovascular disease research*. 2011;2:14-22.

30. Hu G, Vogel SM, Schwartz DE, Malik AB and Minshall RD. Intercellular adhesion molecule-1-dependent neutrophil adhesion to endothelial cells induces caveolae-mediated pulmonary vascular hyperpermeability. *Circ Res*. 2008;102:e120-31.

31. Saliez J, Bouzin C, Rath G, Ghisdal P, Desjardins F, Rezzani R, Rodella LF, Vriens J, Nilius B, Feron O, Balligand JL and Dessy C. Role of caveolar compartmentation in endothelium-derived hyperpolarizing factor-mediated relaxation: Ca2+ signals and gap junction function are regulated by caveolin in endothelial cells. *Circulation*. 2008;117:1065-74.

32. Fan HC, Zhang X and McNaughton PA. Activation of the TRPV4 ion channel is enhanced by phosphorylation. *J Biol Chem*. 2009;284:27884-91.

33. Airan RD, Thompson KR, Fenno LE, Bernstein H and Deisseroth K. Temporally precise in vivo control of intracellular signalling. *Nature*. 2009;458:1025-9.

34. Mineo C, Ying YS, Chapline C, Jaken S and Anderson RG. Targeting of protein kinase Calpha to caveolae. *The Journal of cell biology*. 1998;141:601-10.

35. Martin E, Dahan D, Cardouat G, Gillibert-Duplantier J, Marthan R, Savineau JP and Ducret T. Involvement of TRPV1 and TRPV4 channels in migration of rat pulmonary arterial smooth muscle cells. *Pflugers Arch*. 2012;464:261-72.

36. Ottolini M, Daneva Z, Chen YL, Cope EL, Kasetti RB, Zode GS and Sonkusare SK. Mechanisms underlying selective coupling of endothelial Ca(2+) signals with eNOS vs. IK/SK channels in systemic and pulmonary arteries. *J Physiol*. 2020.

37. Yang XR, Lin MJ, McIntosh LS and Sham JS. Functional expression of transient receptor potential melastatin- and vanilloid-related channels in pulmonary arterial and aortic smooth muscle. *Am J Physiol Lung Cell Mol Physiol*. 2006;290:L1267-76.

38. Xia Y, Fu Z, Hu J, Huang C, Paudel O, Cai S, Liedtke W and Sham JS. TRPV4 channel contributes to serotonin-induced pulmonary vasoconstriction and the enhanced vascular reactivity in chronic hypoxic pulmonary hypertension. *Am J Physiol Cell Physiol*. 2013;305:C704-15.

693 39. Yang XR, Lin AH, Hughes JM, Flavahan NA, Cao YN, Liedtke W and Sham JS. Upregulation of osmo-
694 mechanosensitive TRPV4 channel facilitates chronic hypoxia-induced myogenic tone and pulmonary
695 hypertension. *Am J Physiol Lung Cell Mol Physiol*. 2012;302:L555-68.
696 40. Baxter M, Eltom S, Dekkak B, Yew-Booth L, Dubuis ED, Maher SA, Belvisi MG and Birrell MA. Role
697 of transient receptor potential and pannexin channels in cigarette smoke-triggered ATP release in the
698 lung. *Thorax*. 2014;69:1080-9.
699 41. Rahman M, Sun R, Mukherjee S, Nilius B and Janssen LJ. TRPV4 Stimulation Releases ATP via
700 Pannexin Channels in Human Pulmonary Fibroblasts. *Am J Respir Cell Mol Biol*. 2018;59:87-95.
701 42. Locovei S, Wang J and Dahl G. Activation of pannexin 1 channels by ATP through P2Y receptors
702 and by cytoplasmic calcium. *FEBS Lett*. 2006;580:239-44.
703 43. Thorneloe KS, Cheung M, Bao W, Alsaid H, Lenhard S, Jian MY, Costell M, Maniscalco-Hauk K,
704 Krawiec JA, Olzinski A, Gordon E, Lozinskaya I, Elefante L, Qin P, Matasic DS, James C, Tunstead J, Donovan
705 B, Kallal L, Waszkiewicz A, Vaidya K, Davenport EA, Larkin J, Burgert M, Casillas LN, Marquis RW, Ye G,
706 Eidam HS, Goodman KB, Toomey JR, Roethke TJ, Jucker BM, Schnackenberg CG, Townsley MI, Lepore JJ
707 and Willette RN. An orally active TRPV4 channel blocker prevents and resolves pulmonary edema induced
708 by heart failure. *Science translational medicine*. 2012;4:159ra148.
709 44. Yin J, Hoffmann J, Kaestle SM, Neye N, Wang L, Baeurle J, Liedtke W, Wu S, Kuppe H, Pries AR and
710 Kuebler WM. Negative-feedback loop attenuates hydrostatic lung edema via a cGMP-dependent
711 regulation of transient receptor potential vanilloid 4. *Circ Res*. 2008;102:966-74.
712 45. Alvarez DF, King JA, Weber D, Addison E, Liedtke W and Townsley MI. Transient receptor potential
713 vanilloid 4-mediated disruption of the alveolar septal barrier: a novel mechanism of acute lung injury. *Circ*
714 *Res*. 2006;99:988-95.
715 46. Longden TA, Dabertrand F, Koide M, Gonzales AL, Tykocki NR, Brayden JE, Hill-Eubanks D and
716 Nelson MT. Capillary K(+)-sensing initiates retrograde hyperpolarization to increase local cerebral blood
717 flow. *Nat Neurosci*. 2017;20:717-726.
718 47. Kylhammar D, Bune LT and Radegran G. P2Y(1) and P2Y(1)(2) receptors in hypoxia- and adenosine
719 diphosphate-induced pulmonary vasoconstriction in vivo in the pig. *Eur J Appl Physiol*. 2014;114:1995-
720 2006.
721 48. Li Y, Hu H and O'Neil RG. Caveolae facilitate TRPV4-mediated Ca(2+) signaling and the hierarchical
722 activation of Ca(2+)-activated K(+) channels in K(+)-secreting renal collecting duct cells. *Am J Physiol Renal*
723 *Physiol*. 2018;315:F1626-F1636.
724 49. Zhao YY, Liu Y, Stan RV, Fan L, Gu Y, Dalton N, Chu PH, Peterson K, Ross J, Jr. and Chien KR. Defects
725 in caveolin-1 cause dilated cardiomyopathy and pulmonary hypertension in knockout mice. *Proc Natl Acad*
726 *Sci U S A*. 2002;99:11375-80.
727 50. Zhao YY, Zhao YD, Mirza MK, Huang JH, Potula HH, Vogel SM, Brovkovych V, Yuan JX, Wharton J
728 and Malik AB. Persistent eNOS activation secondary to caveolin-1 deficiency induces pulmonary
729 hypertension in mice and humans through PKG nitration. *J Clin Invest*. 2009;119:2009-18.
730 51. Mercado J, Baylie R, Navedo MF, Yuan C, Scott JD, Nelson MT, Brayden JE and Santana LF. Local
731 control of TRPV4 channels by AKAP150-targeted PKC in arterial smooth muscle. *J Gen Physiol*.
732 2014;143:559-75.
733 52. Sonkusare SK, Dalsgaard T, Bonev AD, Hill-Eubanks DC, Kotlikoff MI, Scott JD, Santana LF and
734 Nelson MT. AKAP150-dependent cooperative TRPV4 channel gating is central to endothelium-dependent
735 vasodilation and is disrupted in hypertension. *Sci Signal*. 2014;7:ra66.
736 53. Moore C, Cevikbas F, Pasolli HA, Chen Y, Kong W, Kempkes C, Parekh P, Lee SH, Kontchou NA, Yeh
737 I, Jokerst NM, Fuchs E, Steinhoff M and Liedtke WB. UVB radiation generates sunburn pain and affects
738 skin by activating epidermal TRPV4 ion channels and triggering endothelin-1 signaling. *Proc Natl Acad Sci*
739 *U S A*. 2013;110:E3225-34.

54. Lohman AW, Leskov IL, Butcher JT, Johnstone SR, Stokes TA, Begandt D, DeLalio LJ, Best AK, Penuela S, Leitinger N, Ravichandran KS, Stokes KY and Isakson BE. Pannexin 1 channels regulate leukocyte emigration through the venous endothelium during acute inflammation. *Nature communications*. 2015;6:7965.

55. Billaud M, Chiu YH, Lohman AW, Parpaite T, Butcher JT, Mutchler SM, DeLalio LJ, Artamonov MV, Sandilos JK, Best AK, Somlyo AV, Thompson RJ, Le TH, Ravichandran KS, Bayliss DA and Isakson BE. A molecular signature in the pannexin1 intracellular loop confers channel activation by the alpha1 adrenoreceptor in smooth muscle cells. *Sci Signal*. 2015;8:ra17.

56. Chen Z, Bakhshi FR, Shajahan AN, Sharma T, Mao M, Trane A, Bernatchez P, van Nieuw Amerongen GP, Bonini MG, Skidgel RA, Malik AB and Minshall RD. Nitric oxide-dependent Src activation and resultant caveolin-1 phosphorylation promote eNOS/caveolin-1 binding and eNOS inhibition. *Mol Biol Cell*. 2012;23:1388-98.

57. Chen X, Qian S, Hoggatt A, Tang H, Hacker TA, Obukhov AG, Herring PB and Seye CI. Endothelial Cell-Specific Deletion of P2Y2 Receptor Promotes Plaque Stability in Atherosclerosis-Susceptible ApoE-Null Mice. *Arterioscler Thromb Vasc Biol*. 2017;37:75-83.

58. Wirth A, Benyo Z, Lukasova M, Leutgeb B, Wettschureck N, Gorbey S, Orsy P, Horvath B, Maser-Gluth C, Greiner E, Lemmer B, Schutz G, Gutkind JS and Offermanns S. G12-G13-LARG-mediated signaling in vascular smooth muscle is required for salt-induced hypertension. *Nat Med*. 2008;14:64-8.

59. Yang Y, Delalio LJ, Best AK, Macal E, Milstein J, Donnelly I, Miller AM, McBride M, Shu X, Koval M, Isakson BE and Johnstone SR. Endothelial Pannexin 1 Channels Control Inflammation by Regulating Intracellular Calcium. *J Immunol*. 2020;204:2995-3007.

60. Vandsburger MH, French BA, Helm PA, Roy RJ, Kramer CM, Young AA and Epstein FH. Multi-parameter in vivo cardiac magnetic resonance imaging demonstrates normal perfusion reserve despite severely attenuated beta-adrenergic functional response in neuronal nitric oxide synthase knockout mice. *Eur Heart J*. 2007;28:2792-8.

61. Ottolini M, Hong K, Cope EL, Daneva Z, DeLalio LJ, Sokolowski JD, Marziano C, Nguyen NY, Altschmied J, Haendeler J, Johnstone SR, Kalani MY, Park MS, Patel RP, Liedtke W, Isakson BE and Sonkusare SK. Local Peroxynitrite Impairs Endothelial Transient Receptor Potential Vanilloid 4 Channels and Elevates Blood Pressure in Obesity. *Circulation*. 2020;141:1318-1333.

Figures.

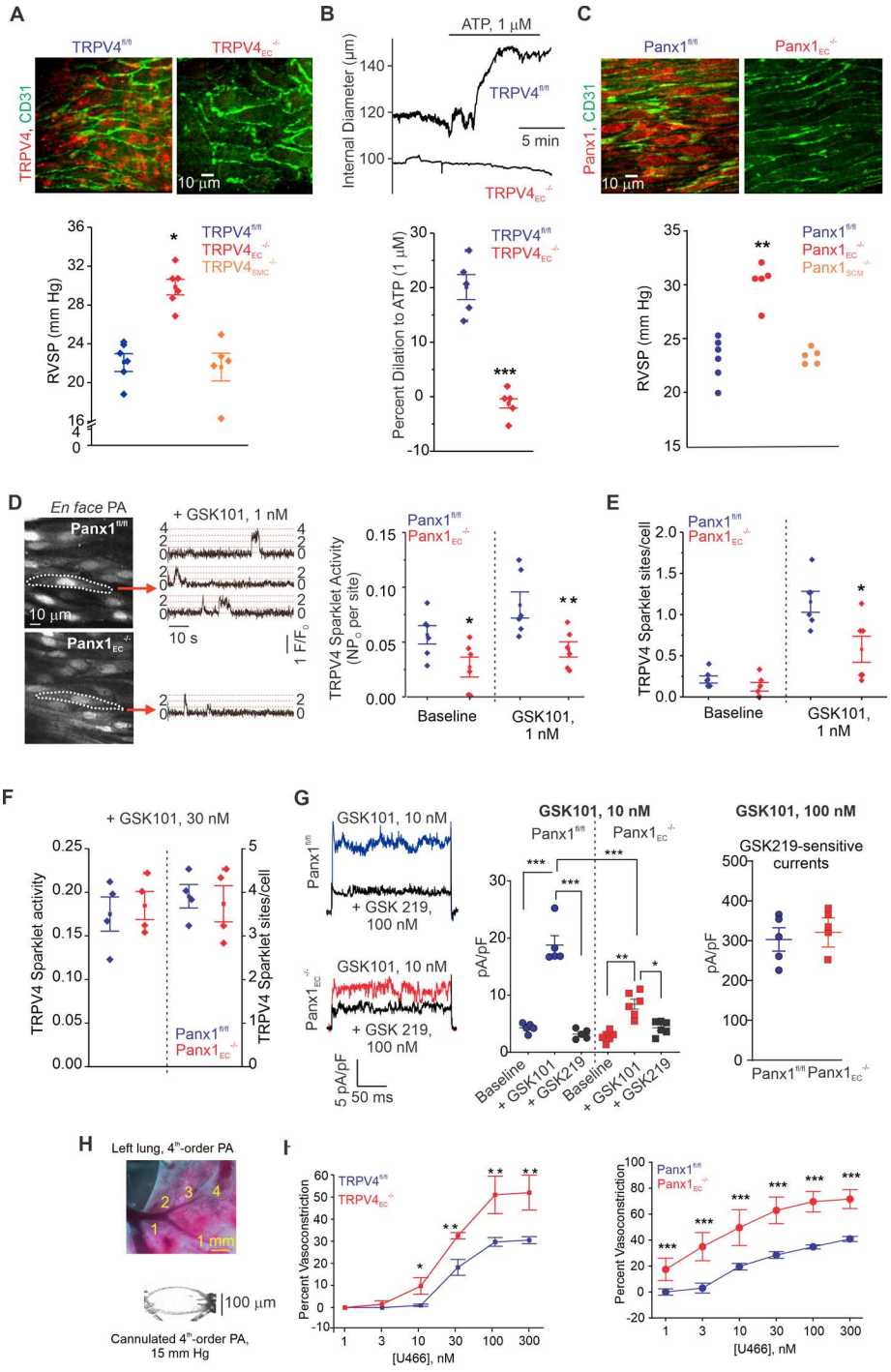

Figure 1. Panx1$_{EC}$–TRPV4$_{EC}$ signaling reduces PA contractility and lowers PAP. A, *top,* Immunofluorescence images of *en face* 4th-order PAs from TRPV4$^{fl/fl}$ (*left*) and TRPV4$_{EC}^{-/-}$ (*right*) mice. CD31 immunofluorescence indicates endothelial cells. *Bottom,* Average resting RVSP

values in $TRPV4^{fl/fl}$, $TRPV4_{EC}^{-/-}$, and $TRPV4_{SMC}^{-/-}$ mice (n = 6; **P* < 0.05 vs. $TRPV4^{fl/fl}$; one-way ANOVA). **B,** *top,* Representative diameter traces showing ATP (1 μmol/L)-induced dilation of PAs from $TRPV4^{fl/fl}$ and $TRPV4_{EC}^{-/-}$ mice, pre-constricted with the thromboxane A2 receptor analog U46619 (50 nmol/L). Fourth-order PAs were pressurized to 15 mm Hg. *Bottom,* Percent dilation of PAs from $TRPV4^{fl/fl}$ and $TRPV4_{EC}^{-/-}$ mice in response to ATP (1 μmol/L; n = 5–10; ****P* < 0.01 vs. $TRPV4^{fl/fl}$ [ATP 1 μmol/L]; t-test). **C,** *top,* Immunofluorescence images of *en face* 4th-order PAs from $Panx1^{fl/fl}$ (*left*) and $Panx1_{EC}^{-/-}$ (*right*) mice. *Bottom,* Average resting RVSP values in $Panx1^{fl/fl}$, $Panx1_{EC}^{-/-}$ and $Panx1_{SMC}^{-/-}$ mice (n = 5; ***P* < 0.01 vs. $Panx1^{fl/fl}$; one-way ANOVA). **D,** *left,* Grayscale image of a field of view of an *en face* preparation of Fluo-4–loaded PAs from $Panx1^{fl/fl}$ and $Panx1_{EC}^{-/-}$ mice showing approximately 20 ECs. Dotted areas indicate $TRPV4_{EC}$ sparklet sites (20 μmol/L CPA + 10 nmol/L GSK101). *Center,* Representative traces showing $TRPV4_{EC}$ sparklet activity in *en face* preparations of PAs from $Panx1^{fl/fl}$ and $Panx1_{EC}^{-/-}$ mice in response to GSK101 (10 nmol/L). Experiments were performed in Fluo-4–loaded PAs in the presence of CPA (20 μmol/L), included to eliminate Ca^{2+} release from intracellular stores. *Right,* $TRPV4_{EC}$ sparklet activity (NP_O) per site in *en face* preparations of PAs from $Panx1^{fl/fl}$ and $Panx1_{EC}^{-/-}$ mice under baseline conditions (i.e., 20 μmol/L CPA) and in response to 1 nmol/L GSK101 (n = 6; **P* < 0.05, ***P* < 0.01 vs. $Panx1^{fl/fl}$; two-way ANOVA). 'N' is the number of channels per site and 'P_O' is the open state probability of the channel. **E,** $TRPV4_{EC}$ sparklet activity, expressed as sites per cell, in *en face* preparations of PAs from $Panx1^{fl/fl}$ and $Panx1_{EC}^{-/-}$ mice under baseline conditions (i.e., 20 μmol/L CPA) and in response to 1 nmol/L GSK101 (n = 6; **P* < 0.05 vs. $Panx1^{fl/fl}$; two-way ANOVA). **F,** $TRPV4_{EC}$ sparklet activity (NP_O) per site and TRPV4 sparklet sites per cell in *en face* preparations of PAs from $Panx1^{fl/fl}$ and $Panx1_{EC}^{-/-}$ mice in response to 30 nmol/L GSK101 (n = 6). **G,** *left,* representative GSK101 (10 nmol/L)–induced

outward $TRPV4_{EC}$ currents in freshly isolated ECs from $Panx1^{fl/fl}$ or $Panx1_{EC}^{-/-}$ mice and effect of GSK2193874 (GSK219, TRPV4 inhibitor, 100 nmol/L) in the presence of GSK101, currents were elicited by a 200 ms voltage step from -50 mV to +100 mV; *center,* scatterplot showing outward currents at +100 mV under baseline conditions, after the addition of GSK101 (10 nM), and after the addition of GSK219 (100 nM), n=5-6 cell, one-way ANOVA, *right*, scatterplot showing GSK219-sensitive $TRPV4_{EC}$ currents in the presence of GSK101 (100 nmol/L; n = 5). **H,** *top,* an image showing the left lung and the order system used to isolate 4th order PAs in this study; *bottom,* an image of a 4th order PA cannulated and pressurized at 15 mm Hg. **I,** *left,* Percent constriction of PAs from $TRPV4^{fl/fl}$ and $TRPV4_{EC}^{-/-}$ mice in response to U46619 (1–300 nmol/L) (n = 5; $*P < 0.05$, $**P < 0.01$ vs. $Panx1^{fl/fl}$; two-way ANOVA). *Right,* Percent constriction of PAs from $Panx1^{fl/fl}$ and $Panx1_{EC}^{-/-}$ mice in response to U46619 (1–300 nmol/L; n = 5; $***P < 0.001$ vs. $Panx1^{fl/fl}$; two-way ANOVA).

828 **Table 1. Fulton Index and Functional MRI analysis of cardiac function in TRPV4$^{fl/fl}$,**
829 **TRPV4$_{EC}^{-/-}$, Panx1$^{fl/fl}$ and Panx1$_{EC}^{-/-}$ mice.** Average Fulton Index, end diastolic and systolic
830 volume (EDV and ESV; μL), ejection fraction (EF; %), stroke volume (SV; μL), R-R interval
831 (ms), and cardiac output (CO; mL/min). Data are presented as means ± SEM (n = 5–8 mice).

	TRPV4$^{fl/fl}$	TRPV4$_{EC}^{-/-}$	Panx1$^{fl/fl}$	Panx1$_{EC}^{-/-}$
Fulton Index	0.22 ± 0.02	0.24 ± 0.01	0.23 ± 0.01	0.26 ± 0.03
EDV (μL)	51.4 ± 5.6	57.4 ± 6.5	46.9 ± 2.7	50.9 ± 2.9
ESV (μL)	21.5 ± 3.5	25.1 ± 4.9	14.8 ± 1.7	13.1 ± 1.4
EF (%)	58.9 ± 2.7	57.4 ± 3.3	68.9 ± 2.0	74.3 ± 2.3
SV (μL)	29.9 ± 2.4	32.3 ± 1.9	32.2 ± 1.3	37.8 ± 2.4
R-R (ms)	124.3 ± 6.0	125.6 ± 6.7	127.1 ± 5.5	130.8 ± 2.5
CO (mL/min)	14.6 ± 1.3	15.5 ± 1.0	15.2 ± 0.6	17.3 ± 1.2

832
833
834
835
836
837
838
839
840

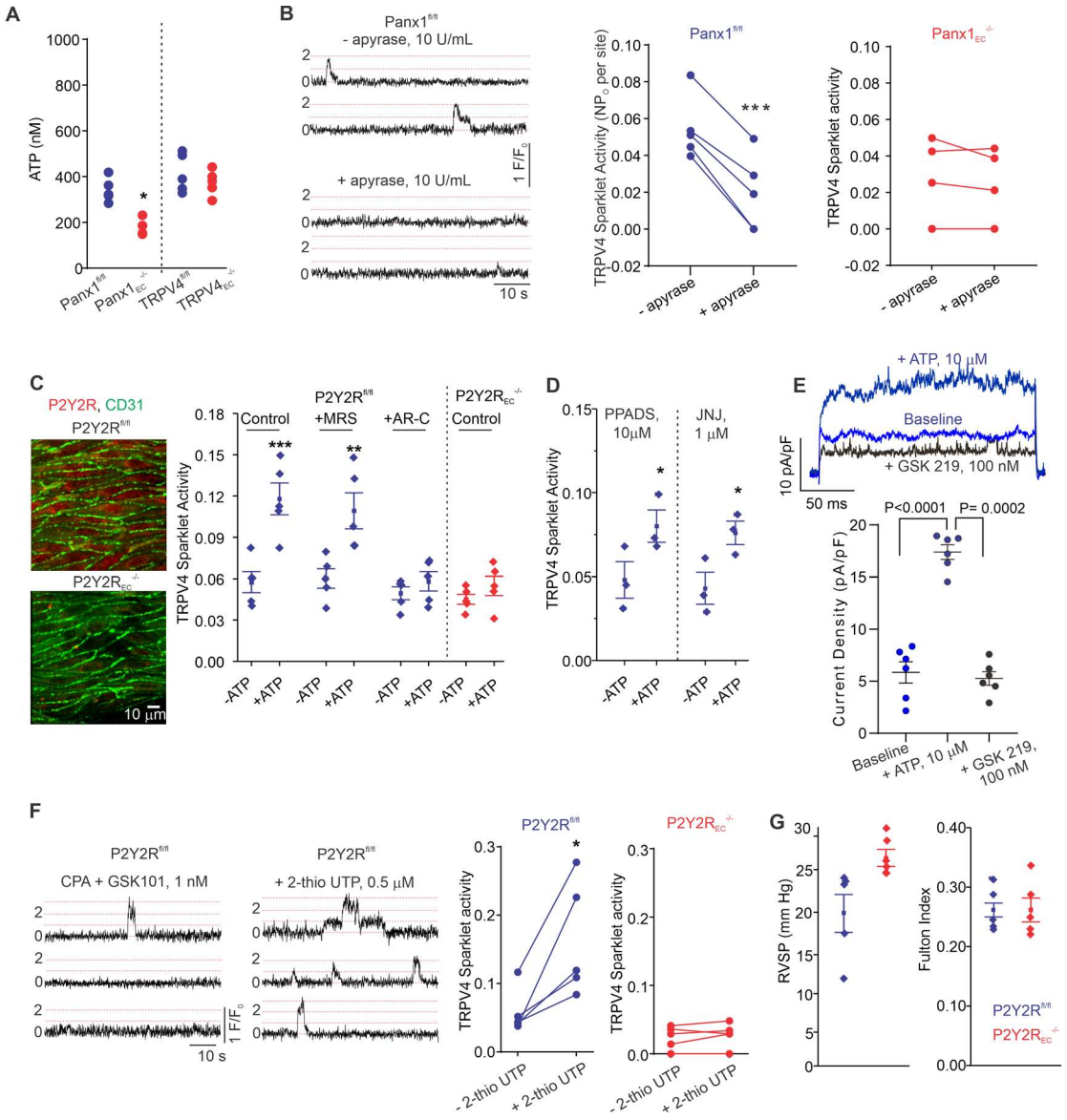

841

842 **Figure 2. eATP activates TRPV4$_{EC}$ channels via P2Y2R$_{EC}$ stimulation. A,** Release of ATP
843 (nmol/L) from PAs of Panx1$^{fl/fl}$, Panx1$_{EC}^{-/-}$, TRPV4$^{fl/fl}$, and TRPV4$_{EC}^{-/-}$ mice (n = 5–6; **P* < 0.05
844 vs. Panx1$^{fl/fl}$; t-test]. **B,** *left,* Representative traces showing TRPV4$_{EC}$ sparklet activity in *en face*
845 preparations of PAs from Panx1$^{fl/fl}$ mice in the absence or presence of apyrase (10 U/mL).
846 Experiments were performed in Fluo-4–loaded PAs in the presence of CPA (20 µmol/L), included
847 to eliminate Ca^{2+} release from intracellular stores. *Right,* TRPV4$_{EC}$ sparklet activity (NP$_O$) per site
848 in *en face* preparations of PAs from Panx1$^{fl/fl}$ and Panx1$_{EC}^{-/-}$ mice in the presence or absence of

apyrase (10 U/mL; n = 5; ***$P < 0.001$ vs. $Panx1^{fl/fl}$ [-apyrase, 10 U/mL]; one-way ANOVA). **C,** *left,* Immunofluorescence images of *en face* 4th-order PAs from $P2Y2R^{fl/fl}$ and $P2Y2R_{EC}^{-/-}$ mice. *Right,* Effects of ATP (10 μmol/L) on $TRPV4_{EC}$ sparklet activity in the absence or presence of the P2Y1R inhibitor MRS2179 (MRS; 10 μmol/L) or P2Y2R inhibitor AR-C 118925XX (ARC; 10 μmol/L) in PAs from $P2Y2R^{fl/fl}$ mice and $P2Y2R_{EC}^{-/-}$ mice, expressed as NP_O per site (n = 5; ***$P < 0.001$, **$P < 0.01$ vs. -ATP; one-way ANOVA). **D,** Effects of ATP (10 μmol/L) on $TRPV4_{EC}$ sparklet activity in the presence of the general P2X1-5/7R inhibitor PPADS (10 μmol/L) and P2X7R inhibitor JNJ-47965567 (JNJ; 1 μmol/L) in PAs of C57BL6/J mice (n = 5; *$P < 0.05$ vs. [-ATP, 10 μmol/L]; one-way ANOVA). **E,** *top,* representative ATP (10 μmol/L)–induced outward TRPV4 currents in freshly isolated ECs from C57BL6 mice and effect of GSK2193874 (GSK219, TRPV4 inhibitor, 100 nmol/L) in the presence of ATP, currents were elicited by a 200 ms voltage step from -50 mV to +100 mV; *bottom,* scatterplot showing outward currents at +100 mV under baseline conditions, after the addition of ATP, and after the addition of GSK219 (100 nM), n=6 cells, one-way ANOVA. **F,** *left,* Representative traces showing $TRPV4_{EC}$ sparklet activity in *en face* preparations of PAs from $P2Y2R^{fl/fl}$ mice in response to CPA (20 μmol/L) + GSK101 (1 nmol/L), CPA + 2-thio UTP (0.5 μmol/L), or CPA + GSK219 (100 nmol/L). *Right,* $TRPV4_{EC}$ sparklet activity (NP_O) per site in *en face* preparations of PAs from $P2Y2R^{fl/fl}$ and $P2Y2R_{EC}^{-/-}$ mice under baseline conditions (i.e., 20 μmol/L CPA) and in response to 2-thio UTP (0.5 μmol/L; n = 5; *$P < 0.05$ vs. $P2Y2R^{fl/fl}$ [-2-thio UTP]; two-way ANOVA). **G**, *left,* Average resting RVSP values in $P2Y2R^{fl/fl}$ and $P2Y2R_{EC}^{-/-}$ mice (n = 6, *$P < 0.05$). *Right,* Average Fulton Index values in $P2Y2R^{fl/fl}$ and $P2Y2R_{EC}^{-/-}$ mice (n = 5–6).

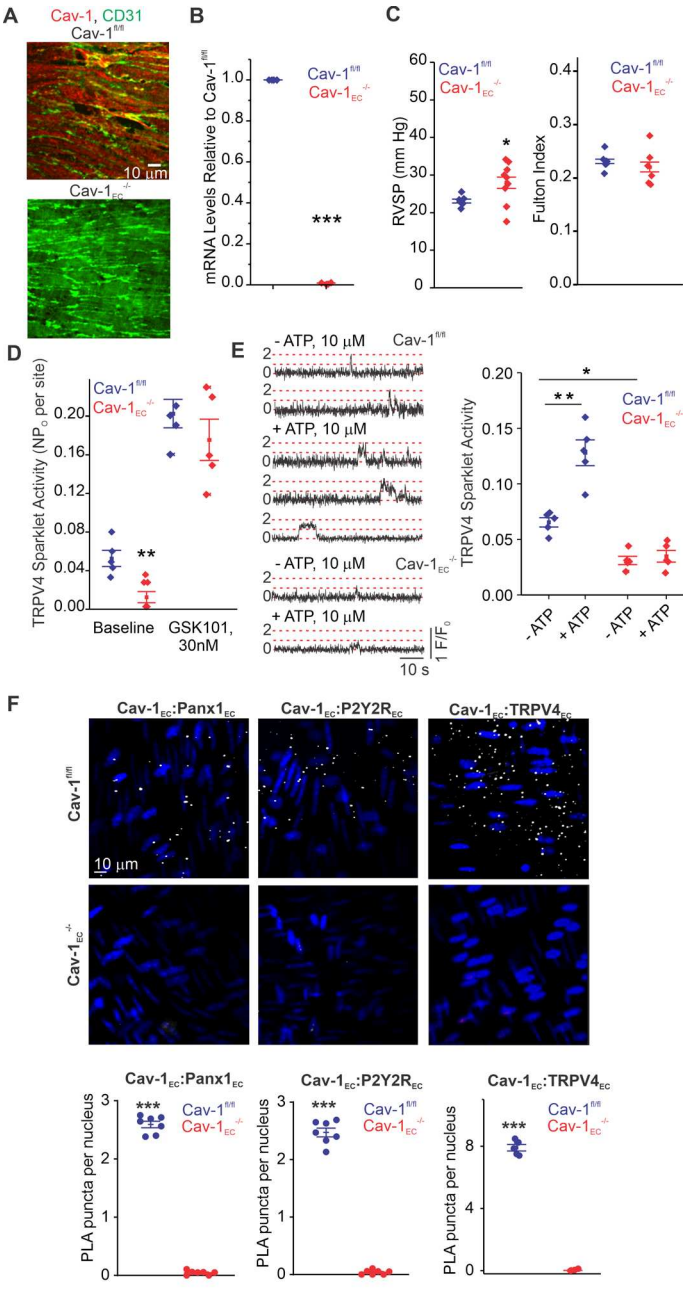

872

873 **Figure 3. Cav-1$_{EC}$ provides a signaling scaffold for Panx1$_{EC}$–P2Y2R$_{EC}$–TRPV4$_{EC}$ signaling**
874 **in PAs. A,** Immunofluorescence images of *en face* 4th-order PAs from Cav-1$^{fl/fl}$ (*top*) and
875 Cav-1$_{EC}^{-/-}$ (*bottom*) mice. **B,** Endothelial Cav-1 mRNA levels in PAs relative to those in Cav-1$^{fl/fl}$
876 mice (n = 4; ***P < 0.001; t-test). **C,** *left,* Average resting RVSP values in Cav-1$^{fl/fl}$ and Cav-
877 1$_{EC}^{-/-}$ mice (n = 6; *P < 0.05 vs. Cav-1$^{fl/fl}$; one-way ANOVA). *Right,* Average Fulton Index values

878 in Cav-$1^{fl/fl}$ and Cav-$1_{EC}^{-/-}$ mice (n = 5–6). **D**, $TRPV4_{EC}$ sparklet activity (NP_O) per site in *en face*
879 preparations of PAs from Cav-$1^{fl/fl}$ and Cav-$1_{EC}^{-/-}$ mice at baseline and in response to 30 nmol/L
880 GGSK101 (n = 6; $^{**}P < 0.01$ vs. baseline Cav-$1^{fl/fl}$; one-way ANOVA). Experiments were
881 performed in Fluo-4–loaded 4^{th}-order PAs in the presence of CPA (20 μmol/L), included to
882 eliminate Ca^{2+} release from intracellular stores. **E**, *left,* Representative traces showing $TRPV4_{EC}$
883 sparklets in *en face* preparations of PAs from Cav-$1^{fl/fl}$ and Cav-$1_{EC}^{-/-}$ mice in the presence and
884 absence of ATP (10 μmol/L). *Right,* $TRPV4_{EC}$ sparklet activity (NP_O) per site in *en face*
885 preparations of PAs from Cav-$1^{fl/fl}$ and Cav-$1_{EC}^{-/-}$ mice in the presence or absence of 10 μmol/L
886 ATP (n = 5; $^{*}P < 0.05$; $^{**}P < 0.01$ vs. [-ATP] Cav-$1^{fl/fl}$; two-way ANOVA). **F,** *top,* Representative
887 merged images of proximity ligation assays (PLA) showing EC nuclei and Cav-1_{EC}:$Panx1_{EC}$, Cav-
888 1_{EC}:$P2Y2R_{EC}$, and Cav-1_{EC}:$TRPV4_{EC}$ co-localization (white puncta) in 4^{th}-order PAs from Cav-
889 $1^{fl/fl}$ and Cav-$1_{EC}^{-/-}$ mice. *Bottom,* Quantification of Cav-1_{EC}:$Panx1_{EC}$, Cav-1_{EC}:$P2Y2R_{EC}$, and Cav-
890 1_{EC}:$TRPV4_{EC}$ co-localization in PAs from Cav-$1^{fl/fl}$ and Cav-$1_{EC}^{-/-}$ mice (n = 5; $^{***}P < 0.001$ vs.
891 Cav-$1^{fl/fl}$; t-test).
892
893
894
895
896
897
898
899

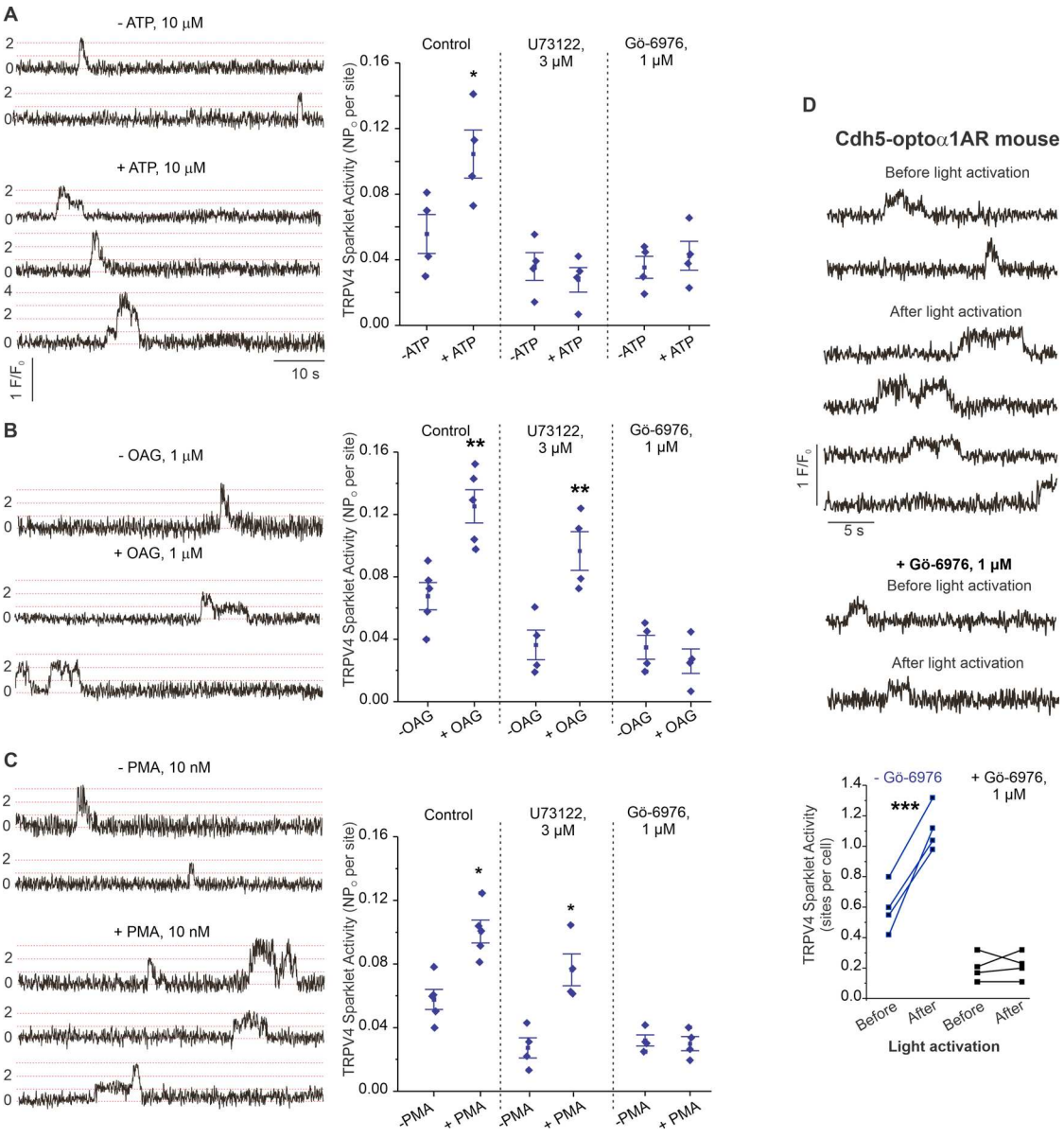

Figure 4. eATP activates TRPV4$_{EC}$ channels via P2Y2R$_{EC}$–PLC–PKC signaling in PAs. A, *left,* Representative traces showing TRPV4$_{EC}$ sparklet activity in *en face* preparations of PAs from C57BL6/J mice before and after treatment with ATP (10 μmol/L). *Right,* Effects of U73122 (PLC inhibitor; 3 μmol/L) or Gö-6976 (PKCα/β inhibitor; 1 μmol/L) on TRPV4$_{EC}$ sparklet activity in *en face* preparations of PAs from C57BL6/J mice before and after treatment with ATP (10 μmol/L), expressed as NP_O per site. Experiments were performed in Fluo-4–loaded 4th-order PAs

in the presence of CPA (20 μmol/L), included to eliminate Ca^{2+} release from intracellular stores (n = 5; $*P < 0.05$ vs. [-ATP]; one-way ANOVA). **B,** *left,* Representative traces showing $TRPV4_{EC}$ sparklet activity in *en face* preparations of PAs from C57BL6/J mice in the absence or presence of OAG (DAG analogue; 1 μmol/L). *Right,* Effects of U73122 (3 μmol/L) or Gö-6976 (1 μmol/L) on $TRPV4_{EC}$ sparklet activity in *en face* preparations of PAs from C57BL6/J mice before and after treatment with OAG (1 μmol/L), expressed as NP_O per site (n = 6; $^{**}P < 0.01$ vs. [-OAG]; one-way ANOVA). **C,** *left,* Representative traces showing $TRPV4_{EC}$ sparklets in *en face* preparations of PAs from C57BL6/J mice in the absence or presence of PMA (PKC activator; 10 nmol/L). *Right,* Effects of U73122 (3 μmol/L) or Gö-6976 (1 μmol/L) on $TRPV4_{EC}$ sparklet activity in *en face* preparations of PAs from C57BL6/J mice before and after treatment with PMA (10 nmol/L), expressed as NP_O per site (n = 6; $*P < 0.05$ vs. [-PMA]; one-way ANOVA). **D.** *top,* Representative traces showing $TRPV4_{EC}$ sparklet activity in *en face* preparations of PAs from Cdh5-optoα1AR (adrenergic receptor) mouse before and after the light activation (470 nm); *bottom*, scatter plot showing the sparklet activity, expressed as sparklet sites per cell, before and after the light activation, in the absence or presence of PKCα/β inhibitor Gö-6976 (1 μM, n=4, $***P < 0.001$).

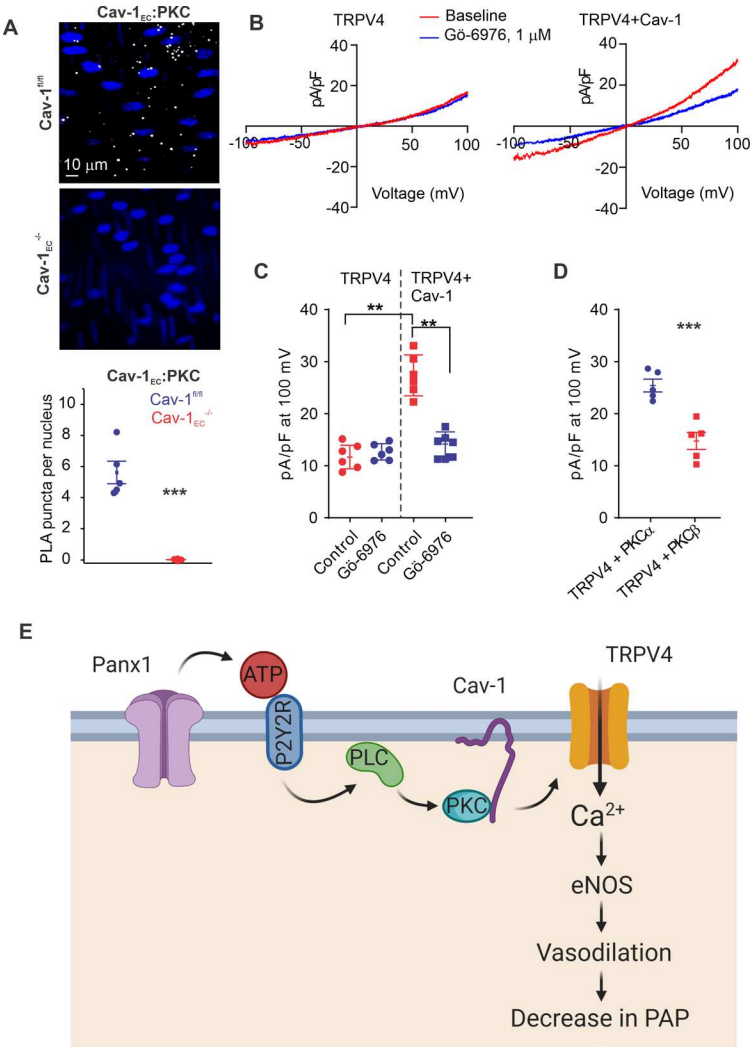

929

930 **Figure 5. Localization of PKCα with Cav-1$_{EC}$ increases the activity of TRPV4$_{EC}$ channels. A,**

931 *top,* Representative merged images of proximity ligation assays (PLA) showing EC nuclei and

932 Cav-1:PKC co-localization (white puncta) in 4th-order PAs from Cav-1$^{fl/fl}$ and Cav-1$_{EC}^{-/-}$ mice.

933 *Bottom,* Quantification of Cav-1:PKC co-localization in PAs from Cav-1$^{fl/fl}$ and Cav-1$_{EC}^{-/-}$ mice (n

934 = 5; ***$P < 0.001$ vs. Cav-1$^{fl/fl}$; t-test). **B,** Representative traces showing TRPV4 currents in the

935 absence or presence of Gö-6976 (PKC inhibitor; 1 μmol/L) in HEK293 cells transfected with

936 TRPV4 only or co-transfected with TRPV4 plus wild-type Cav-1, recorded in the whole-cell

937 patch-clamp configuration. **C,** Current density plot of TRPV4 currents at +100 mV in the absence

938 or presence of Gö6976 (1 μmol/L) in HEK293 cells transfected with TRPV4 or TRPV4 + Cav-1
939 (n = 5; $^{**}P < 0.01$ vs. Control; one-way ANOVA). **D,** Current density plot of TRPV4 currents at
940 +100 mV in HEK293 cells transfected with TRPV4 + PKCα or TRPV4 + PKCβ (n = 5; $^{***}P <$
941 0.001 vs. TRPV4 + PKCα; t-test). **E,** Schematic depiction of the $Panx1_{EC}$–$P2Y2R_{EC}$–$TRPV4_{EC}$
942 signaling pathway that promotes vasodilation and lowers PAP in PAs. ATP released from $Panx1_{EC}$
943 channels activates $P2Y2R_{EC}$ purinergic receptors on the EC membrane. Stimulation of $P2Y2R_{EC}$
944 recruits PKCα, which anchors to the scaffolding protein $Cav\text{-}1_{EC}$ in close proximity to $TRPV4_{EC}$
945 channels. $TRPV4_{EC}$ channel-dependent vasodilation lowers pulmonary arterial pressure (PAP).
946
947
948
949